NASA Contractor Report 201614

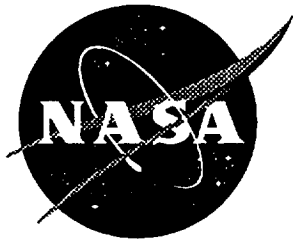

A Fundamental Study of Laser Beam Welding Aluminum-Lithium Alloy 2195 for Cryogenic Tank Applications

R. P. Martukanitz and R. Jan
Pennsylvania State University, Applied Research Laboratory
State College, Pennsylvania

Grant NAG1-1554

September 1996

National Aeronautics and
Space Administration
Langley Research Center
Hampton, Virginia 23681-0001

ABSTRACT

Based on the potential for decreasing costs of joining stiffeners to skin by laser beam welding, a fundamental research program was conducted to address the impediments identified during an initial study involving laser beam welding of aluminum-lithium alloys. Initial objectives of the program were the identification of governing mechanism responsible for process related porosity while establishing a multivariant relationship between process parameters and fusion zone geometry for laser beam welds of alloy 2195 (Al-4.0Cu-1.0Li-0.4Mg-0.4Ag). A 14 kW CO_2 laser and the Laser Articulating Robotic System were used to produce all laser beam welds. The lap-joint configuration utilized during the study entailed welding 1.25 mm (0.050 in.) thick 2195-T6 to 3.12 mm (0.125 in.) thick 2195-T8 and was selected to simulate stiffeners to skin for stiffened panel applications.

Transmission electron microscopy was performed to characterize the 2195-T8 base material and heat affected zone. The base metal microstructure of this alloy in the peak aged temper was found to be dominated by T_1 (Al_2CuLi) and θ' (Al_2Cu) precipitates. The gradual loss of strength for positions representing the heat affected zone is believed to be attributed to dissolution of the T_1 precipitate. A narrow region of the heat affected zone that is adjacent to the fusion zone interface may influence weld toughness by the presence of precipitate free zones and solute depletion.

A three-level fractional factorial experiment was conducted to establish quantitative relationships between primary laser beam processing parameters and critical weld attributes. Strong statistical correlation was observed for : weld penetration as a function of welding velocity and stand-off distance, weld width at the interface as a function of stand-off distance, and porosity rating as a function of amount removed by chemical milling and welding velocity. Parameters identified for optimal conditions were: an output power of 10 kW, a processing speed of 10.6 cm/s (250 IPM), a stand-off distance of 13.3 cm (5.25 in.), and chemical milling of 0.25 mm (0.010 in.) per side prior to welding. These parameters were utilized during a reproducibility study to ascertain process consistency. Although process consistency appeared high for welds produced during partial completion of this study, numerous cracks on the top-surface of the welds were discovered during visual inspection and necessitated additional investigations concerning weld cracking.

A crack sensitivity study was performed to identify possible means of reducing or eliminating cracks within the laser beam welds of 2195. Two experiments were conducted to assess the effect of filler alloy additions on crack sensitivity: the first experiment was used to ascertain the effects of various filler alloys on cracking and the second experiment involved modification to process parameters for increasing filler metal dilution. Filler alloys 2319 (Al-6.3 Cu), 4043 (Al-5.3Si), 4047 (Al-12Si), 4145 (Al-10Si-4Cu), and 5356 (Al-5.0Mg) were evaluated for reducing crack susceptibility. Process parameters used during this experiment were identical to those established during the parametric study, except for the addition of filler metal. Results indicated that filler alloys 4047 and 4145 showed promise for eliminating weld cracking; however, increased filler metal dilution was believed to be necessary for eliminating cracking. Increased dilution would require modifications to the established process parameters. Process parameters were identified for increasing filler metal dilution but maintaining weld penetration requirements. Parameters that provided the minimal amount of cracking while controlling penetration into the skin-sheet were 10.3 kW of power, 7.9 cm/s (150 IPM) travel speed, stand-off distance of 1.55 mm (0.062 in.) above focus, and a wire feed speed of 15.8 cm/s (300 IPM). Although the frequency of solidification cracks was reduced with these parameters, solidification cracking could not be eliminated. Parameters that resulted in increased levels of filler addition were also found to be contrary to the parametric window established for optimizing weld profile and pool stability. Although weld cracking was not eliminated, two panels representing laser beam lap-welds were produced using 4047 filler metal and the modified process parameters for abbreviated mechanical property testing at NASA Langley Research Center.

TABLE OF CONTENTS

LIST OF FIGURES

LIST OF FIGURES - Continued

LIST OF TABLES

1.0 INTRODUCTION

Results of a prior investigation sponsored by NASA Langley Research Center and conducted by the Applied Research Laboratory, Pennsylvania State University (ARL Penn State) have shown that laser beam welding offered several potential advantages over resistance spot welding for producing "built-up" structures from aluminum-lithium alloys for cryogenic tankage applications. These included: dramatically higher processing speeds, improved load transfer between stiffeners and skin, lower cost, and processing in a fully automated environment (Ref. 1). One form of such a structure is shown Figure 1.

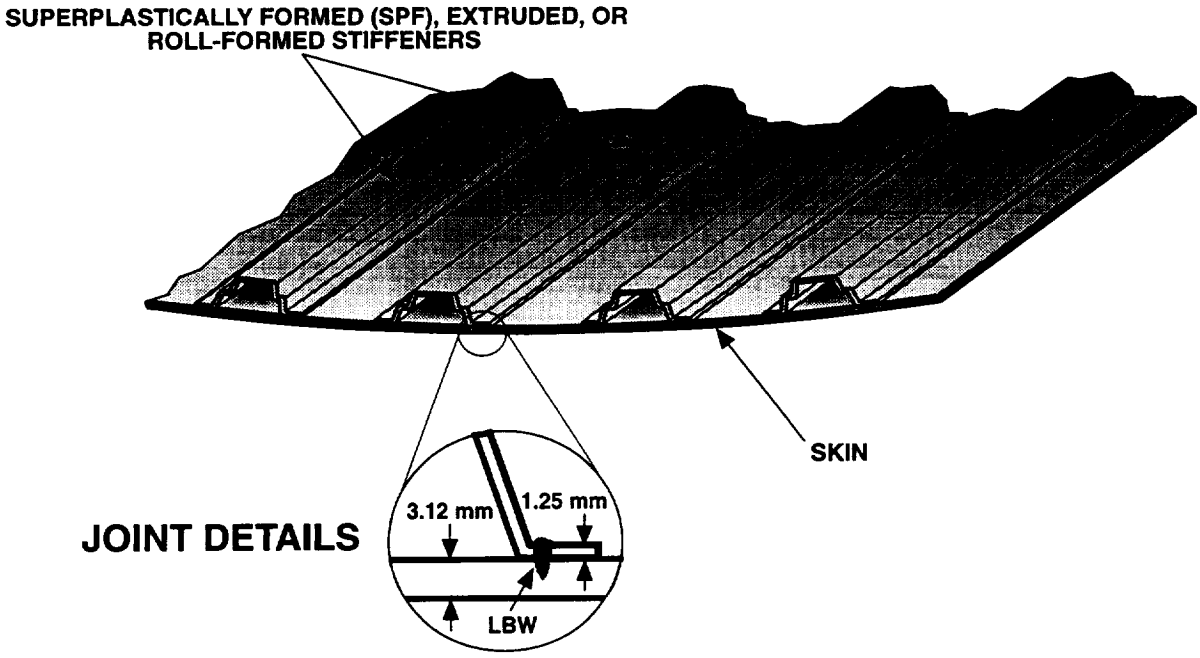

Figure 1 - Schematic of Built-up Structure that may Utilize Laser Beam Welding to Join Stiffeners to Skin.

Results of this investigation indicated that laser beam welding could provide improved productivity and lower costs over resistance welding for fabrication of stiffened panels. Laser beam welding involves the use of a highly focused beam of coherent light directed at the component to be welded by the use of mirrors or lenses. The highly focused beam produces an intense heat source enabling deep penetration and extremely high processing speeds. An inert gas, typically helium, is supplied externally to suppress the formation of plasma formed by volatilization of material and to shield the molten pool from contamination. Lap-welds having good penetration and positive weld bead reinforcement were produced by autogenously laser beam welding at power levels of 5 to 7 kW and travel speeds of 6.4 to 6.8 cm/s (150 to 160 IPM); speeds considerably higher than that capable with resistance welding. Conditions amicable to improved load transfer and enhanced structural integrity were also demonstrated by the laser beam welding process. Laser beam welding provided accessibility such that lap-welds could be produced very near the edge of the vertical member on

stepped-hat stiffeners of prototype panels. Tensile tests of laser beam welds representing partial penetration of the skin provided a joint efficiency of 77 percent (at 40 percent through-thickness penetration) for 2090-T83 and 65 percent joint efficiency (at 60 percent through-thickness penetration) for 2095-T8. It was also found during this evaluation that the average shear strength of laser beam welds between 2095-T6 to 2095-T8 was 130 MPa (18.8 KSI), as compared to an average shear strength of 81 MPa (11.7 KSI) for 8090-T6 laser beam welded to 2090-T83.

Although the results of the investigation supported the potential advantages of laser beam welding for producing stiffened panels, limitations concerning current processing were also identified. Aggressive pretreatment in the form of chemical milling in a 32 percent NaOH aqueous solution at 99 °C (210 °F) was found to be necessary to reduce porosity at the weld interface. This required removal of 0.25 mm (0.010 in.) per side by chemical milling prior to welding and was believed due to the presence of a hydrogen-enriched layer near the surface. Prior investigations had shown that thermal processing of aluminum-lithium alloys result in surface reactions between the metal and water vapor to form diatomic hydrogen (Refs. 2-4). Hydrogen is subsequently absorbed into the surface and may be available to form lithium hydride. The result is the formation of a hydrogen enriched and lithium depleted zone near the surface of these material. Shown in Figure 2 is the concentration of lithium by atomic absorption measurements of NaOH solutions used to chemically mill 3.0 mm (0.120 in.) thick 2090-T83 and 2095-T8 specimens that were utilized during an earlier investigation (Refs. 5&6). The figure illustrates the increasing lithium content associated with the surface of these alloys that were chemically milled. The lithium depleted zone is represented by lower levels of lithium associated with the chemical milling solutions used to remove material from the surface.

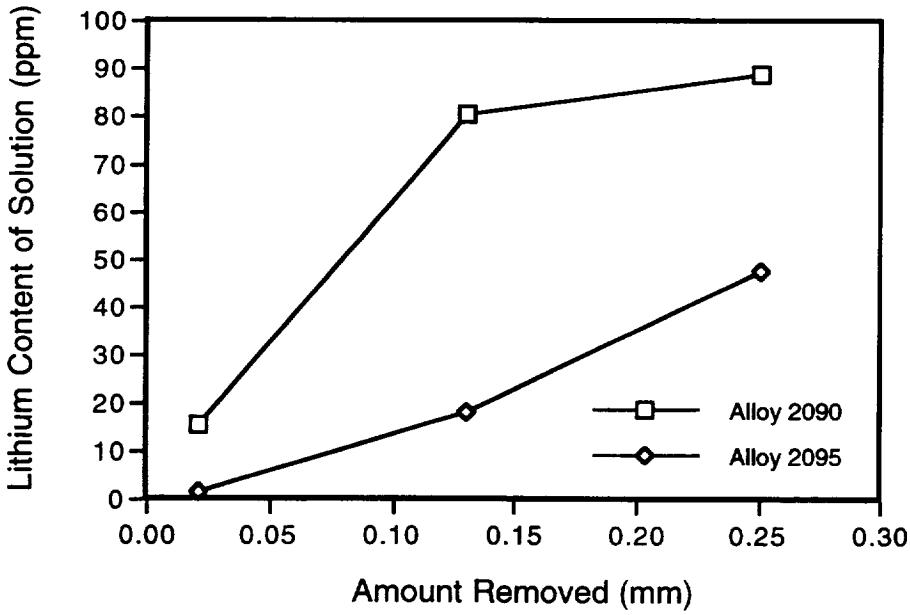

Figure 2 - Results of Atomic Absorption Measurements for Lithium Content of NaOH Solutions Used to Chemically Mill Alloys 2090 and 2095 to Various Depths (Ref. 5).

Although chemical milling was able to reduce porosity at the interface between the stiffeners and skin, radiographic analysis indicated that weld porosity was consistently observed at the root of the welds. Metallographic analysis also indicated that the porosity may have been process related rather than being associated with a hydrogen source based on the position and shape of the pores within the root of the laser beam welds . During laser beam welding, the material under the beam evaporates and forms a cavity referred to as a keyhole. As the heat source moves along the base material the keyhole continually melts material at the front edge with solidification occurring at the rear. The keyhole is maintained by balancing the hydrodynamic forces of the pool with the vapor pressure within the cavity. Although a complete treatise does not exist, results of prior investigations have indicated that vaporization of volatile alloying elements, such as magnesium and lithium, and keyhole instability may be responsible for process related porosity during laser beam welding of aluminum (Refs. 7-9).

Also, the lap weld configuration utilized for the joints required optimal shear load-carrying capability between the stiffener and skin. The extent to which a lap weld is capable of carrying shear loads is a function of both the strength of the metallurgical structure of the fusion zone and interface area in the plane of loading. Laser beam welding parameters utilized during the earlier study were primarily chosen to ensure penetration into the skin. Although adequate penetration was obtained, the resultant welds exhibited high depth-to-width ratios typically associated with laser beam welds. Increasing the width of the weld was expected to result in greater shear area at the stiffener-to-skin interface and provide greater shear load-carrying capability. Defocusing of the laser beam was suggested as a method of providing greater width of the weld at the interface. The addition of filler metal during laser beam welding was also suggested as a means of improving pool stability and possibly reducing porosity.

1.1 Objective of Research Effort

Based on the potential for decreasing costs for joining of stiffeners to skin by laser beam welding, a fundamental research effort was initiated to address the impediments identified during the initial study. The program would involve the current aluminum-lithium alloy of interest, i.e. alloy 2195 (Al-4.0Cu-1.0Li-0.4Mg-0.4Ag). Objectives of the program were the identification of governing mechanisms responsible for process related porosity while establishing a multivariant relationship between process parameters and fusion zone geometry. The approach would involve the use of a designed experiment methodology to measure the synergistic effects of process parameters on weld porosity and fusion zone geometry. This understanding would then be applied to improve the laser beam welding process for aerospace applications by minimizing weld porosity and optimizing fusion zone geometry based on load-carrying capability. Specific tasks of the program would include: a fundamental characterization of the alloy 2195 base material, a parametric study of processing parameters on weld attributes, and a reproducibility study to determine process consistency.

2.0 BASE METAL CHARACTERIZATION

The strength of the face sheet in the vicinity of the partial penetration weld of the stiffener for alloy 2195 is dictated by the interaction of local stress states on microstructures developed or evolved in various regions of the weld. The microstructure of the fusion zone is primarily governed by transformations occurring during solidification; whereas, microstructures within the heat affected zone are determined by solid state reactions of the original base-metal microstructure. The objective of this task was to characterize the base metal microstructure and better understand the microstructural transformations within the heat affected zone of alloy 2195. This information would be used to ascertain the effects of these transformations on joint mechanical properties.

Aluminum alloys containing Cu and Li possess a wide variety of precipitates. Precipitates representing equilibrium phases in this ternary system include θ , T_1 (Al_2CuLi), T_2 (Al_6CuLi_3), and T_B ($Al_{7.5}Cu_4Li$). However, the operative strengthening phases in commercial alloys containing Cu and Li are determined by the level of alloying additions, the presence of minor constituents, and the precipitation heat-treating practice (Refs. 10-17). At high Cu/Li ratios, such as with alloy 2195, T_1 and θ' represent the dominant strengthening phases. Both T_1 and θ' form as semi-coherent plates along preferred orientations of the matrix. The T_1 precipitates grow on the four-variants of the {111} planes of the matrix and θ' grows on the three-variants of the {100} planes. Alloys containing relatively small amounts of Mg, as alloy 2195, may also exhibit S' (Al_2CuMg) which forms as semi-coherent rods along the <100> directions of the matrix. Also, all commercial Al-Cu-Li alloys include small levels of Zr that form fine, metastable β' (Al_3Zr) particles which act to retard recrystallization and grain growth.

2.1 Microstructural Characterization

Transmission electron microscopy (TEM) was used to characterize microstructures representing 2195-T8 base metal, as well as transformation governing loss of strength within the heat affected zones. Base material and variable polarity plasma arc welds on 5.0 mm (0.200 in.) thick 2195-T8 was obtained from Lockheed Martin Corporation's Manned Space Systems Division, Huntsville, Al. This material was used so that full-thickness specimens could be removed at precise positions within the heat affected zone for TEM. Thermal analysis utilizing a heat transfer model developed for aluminum was used to estimate thermal profiles associated with the representative TEM specimens.

Thermal analyses were conducted to represent the one-pass, variable polarity plasma arc welds of 5.0 mm (0.200 in.) thick 2195-T8 alloy produced with 2319 filler wire and provided by Lockheed Martin Corporation. The explicit finite differencing method was utilized to simulate cross-sectional isotherms and transient temperatures associated with the variable polarity plasma arc welding under the quasi-steady state conditions . The model uses the forward time, center differencing technique to simulate conductive heat transfer, and associated surface heat losses by convection and radiation, of a three dimensional plate and a moving heat source. Thermophysical properties of alloy 2195 were estimated to be: 543°C solidus temperature, 643°C liquidus temperature, 0.243 cal/cm-s-°C thermal conductivity, 2.71 g/cm^3 density, 0.240 cal/gm-°C specific heat, and 95.0 cal/g latent heat of fusion. The welding parameters used to produce the weld at Lockheed Martin Corporation's Huntsville facility were used as input for the simulations. The welding parameters were: 125 amperes, 22.3 volts, and 0.415 cm/s (9.8 IPM) travel speed. An iterative procedure involving the calibration of the model predictions under the quasi-steady state condition to actual weld profile was used to determine process efficiency. A process efficiency of 60 percent

provided the best fit of experimental and observed data and was employed during transient analysis. Because the heat transfer model assumes thermal loading of the top surface, which is not the case for variable polarity plasma arc welding, some inconsistencies were observed between measured and predicted weld profiles. The 60 percent efficiency represents correlation of the measured weld profile and the predicted solidus isotherm near the center of the plate thickness. Figure 3 (a) depicts the comparison of weld profiles and predicted isotherms during quasi-steady state analysis, and Figure 3 (b) shows the predicted thermal profiles for various distances from the weld center line for the quasi-steady state condition.

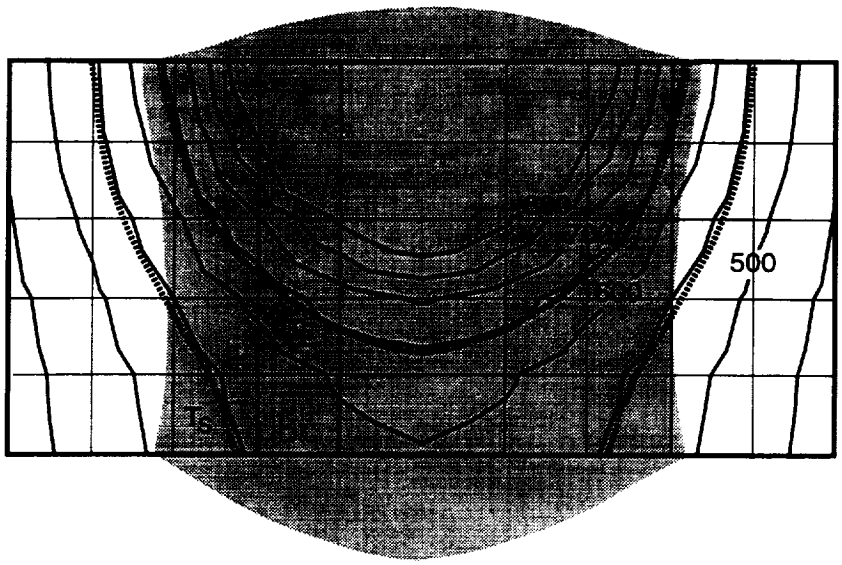

(a) Comparison of actual variable polarity plasma arc weld profile to simulated isotherms.

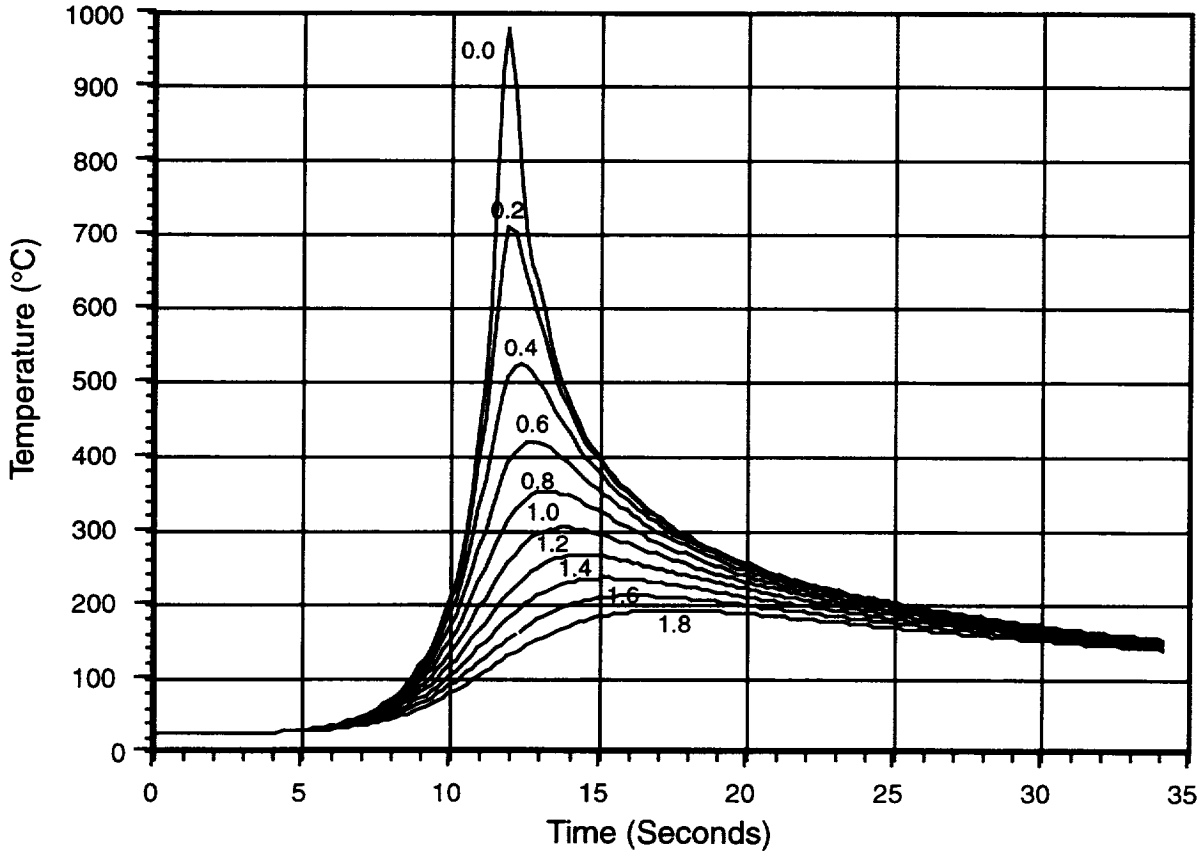

(b) Simulated thermal transients at various distances from weld centerline for variable polarity plasma arc weld (distances from centerline in cm).

Figure 3 - Results of Heat Transfer Simulations of Variable Polarity Plasma Arc Weld obtained from Lockheed Martin Corporation.

Samples were precisely removed at predetermined positions from the heat affected zone of 5.0 mm (0.200 in.) thick 2195-T8 welded with the VPPA process. Samples were removed parallel to the welding direction using a diamond blade wafering saw at a low speed while utilizing cutting lubricant. The location of the samples in relation to the weld were: 1.0 mm (0.040 in.) from the fusion zone interface, 7.0 mm (0.280 in.) from the fusion zone interface, 12.0 mm (0.480 in.) from the fusion zone interface, and 60 mm (2.40 in.) from the interface and representing the base metal microstructure. The position, strength, and peak temperature represented by these specimens are shown in Figure 4 (Ref. 18). Approximate yield strength values were obtained by conversion of microhardness measurements (Ref. 19).

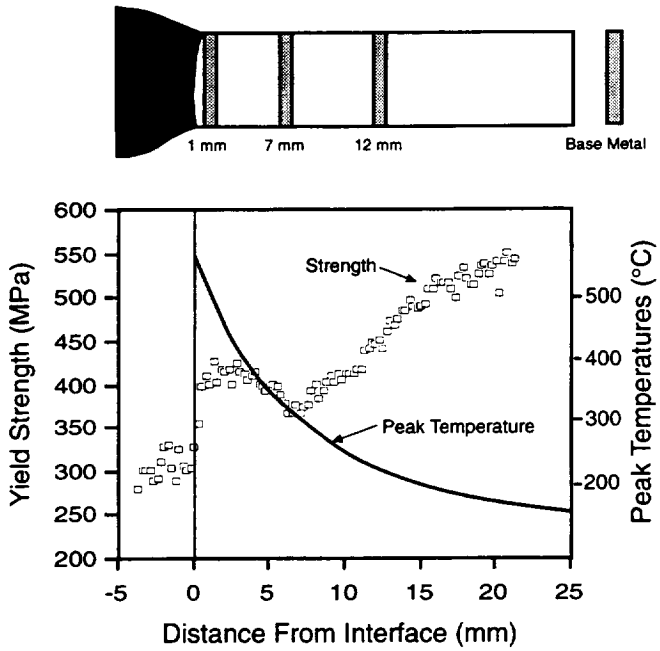

Figure 4 - Position, Strength, and Peak Temperatures Represented by Transmission Electron Microscopy Specimens of Variable Polarity Plasma Arc Weld of Alloy 2195-T8.

TEM specimens were prepared by grinding both sides using a Struers Planopol-3 and Pedemax-2 automated grinding machine with 1200 and 2400 grit silicon-carbide paper and water to an approximate thickness of 125 μm (0.005 in.). Specimens were then punched to a 3 mm diameter and hand ground with 4000 grit silicon-carbide paper and water to a thickness of approximately 50 μm (0.002 in.). These specimens were further thinned by twin jet electropolishing in a 25% Nital solution cooled to -20 ± 5°C (-4 ±9°F) using a potential of 12 V. The time required to achieve a through-hole was approximately 1 minute (± 15 sec.) at a jet speed setting of 3.0. After thinning, specimens were ion milled at 1 mA and 3.5 kV for approximately 30 minutes to remove any residue from the electropolishing process. The majority of electron microscopy was performed on a Philips EM420 transmission electron microscope operating at 120 kV; however, limited high resolution transmission electron microscopy was also performed on a Hitachi HF-2000 Cold Field Emission Analytical transmission electron microscope at the High Temperature Materials Laboratory at Oak Ridge National Laboratory.

Utilizing the habit plane orientations of the precipitates, bright field and centered dark field images were obtained with the use of selected area diffraction patterns. Figure 5 represents transmission electron micrographs of the base metal. The micrographs indicate the primary strengthening precipitates of the 2195-T8 base metal to be T_1 and θ'. Both of these precipitates exhibit a plate-like morphology, with θ' aligned along the {100} planes and T_1 being aligned along the {111} planes of the matrix. The centered dark field image of 5(a) illustrates two variants of the θ' phase on the {100} planes. Figure 5(b) represents the bright field and dark field images of the T_1 phase present within the 2195-T8 base metal. One variant of T_1 is shown in the figure.

Figure 6 shows representative transmission electron micrographs of material obtained from a position 12 mm from the fusion zone interface and has experienced peak temperatures of approximately 220°C (428°F). The strength in this region has decreased approximately 28% when compared to the original base metal strength. The micrographs of specimens obtained from this region show that θ' has been completely dissolved at this temperatures but the presence of T_1 remains. Based on the projected image, the diameter and number density of the T_1 plates have decreased.

The micrographs of Figure 7 represent a position within the heat affected zone that was 7 mm from the fusion zone interface, and is characterized by peak temperatures of approximately 320°C (608°F). This position also represents the lowest strength obtained within the heat affected zone. This trough or minimum in strength within the heat affected zone is typical of many aluminum alloys that are precipitation strengthened. The projected dark field image of Figure 7 indicates plate diameters similar to that of the base metal but precipitate number density comparable to the microstructure at 12 mm from the fusion zone interface. As mentioned earlier, the θ' phase had completely dissolved at relatively low temperatures, and hence, is not present at this position.

Figures 8 and 9 shows transmission electron micrographs representing a position 1 mm from the fusion zone interface. This position has experienced peak temperatures approaching 500°C (932°F) and has resulted in considerable coarsening of the T_1 phase at low-angle sub-boundaries. Strength within this region is similar to that of as-quenched material. Small amounts of β' particles are also observed in the bright field image. The β', which has a composition of Al_3Zr, exhibits a spherical morphology. The mottled appearance in the background of the bright field image of Figure 8 also suggest the presence of Guinier-Preston Zones (GP zones) that have also formed upon cooling. The supposition concerning the presence of GP zones within this region is further supported by the micrograph of Figure 9 along with the corresponding selected area diffraction pattern. Evident in the diffraction pattern is streaking along the <100> directions of the matrix which indicates the presence of Cu containing zones similar to those found in Al-Cu alloys. The formation of GP zones has been reported in variants of alloy 2195 after solutionizing and quenching (Ref. 20). The region adjacent to the fusion zone interface may be characterized by rapid heating to peak temperatures, that resulted in complete dissolution, and cooling. However, relatively low cooling rates promote heterogeneous nucleation and growth at grain boundaries and the possibility of precipitate free zones (PFZs) adjacent to the boundaries. This phenomena has been observed in aluminum alloys containing Cu or Li and is due to volume diffusion of solute to grain boundaries followed by rapid diffusion along the boundaries (Ref. 21&22).

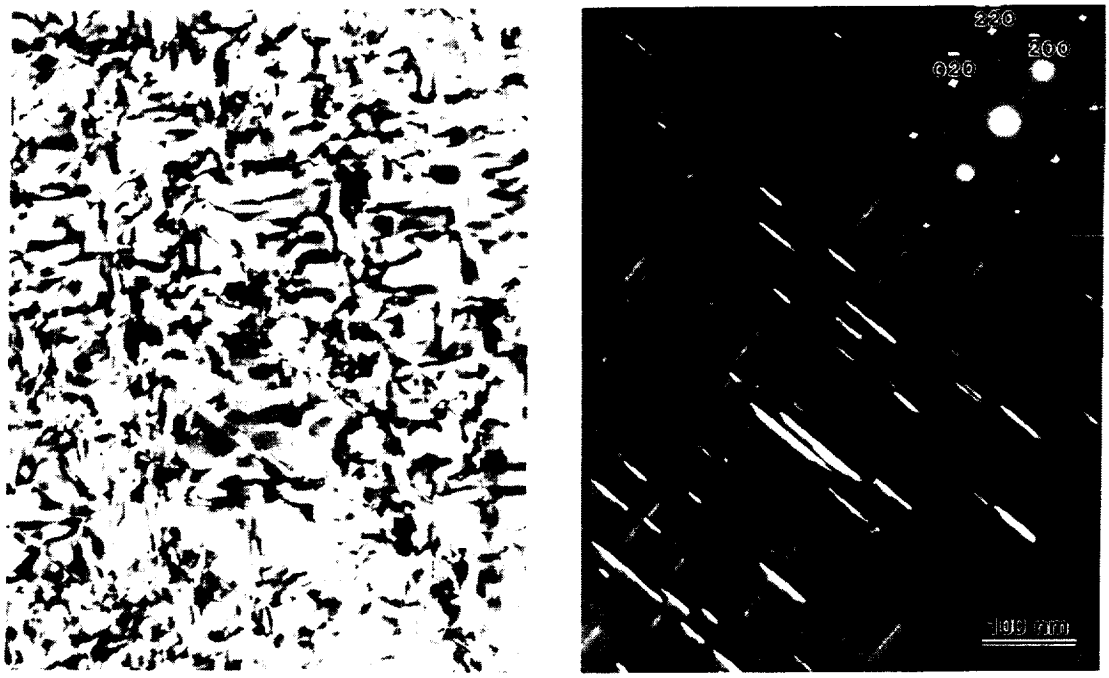

Bright Field Image

Centered Dark Field Image

(a)

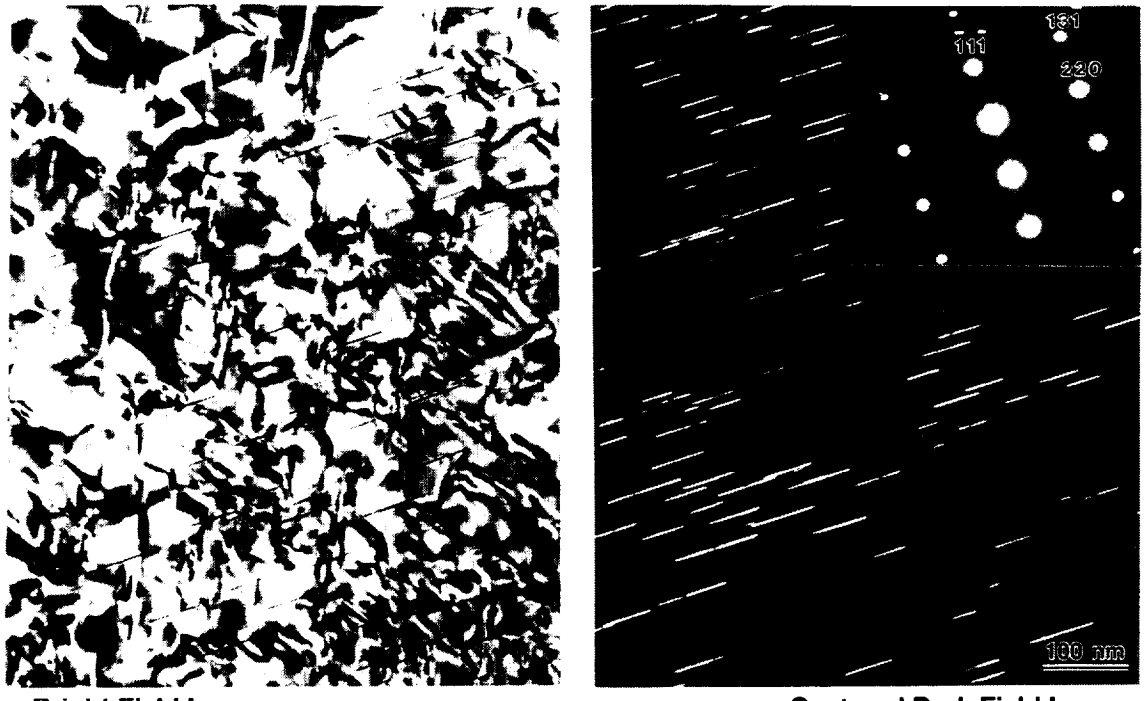

Bright Field Image

Centered Dark Field Image

(b)

Figure 5 - Transmission electron micrographs of 2195-T8 base metal showing (a) two variants of θ' (Al_2Cu) as plates on the {100} planes of the matrix and (b) T_1 (Al_2CuLi) plates on the {111} planes.

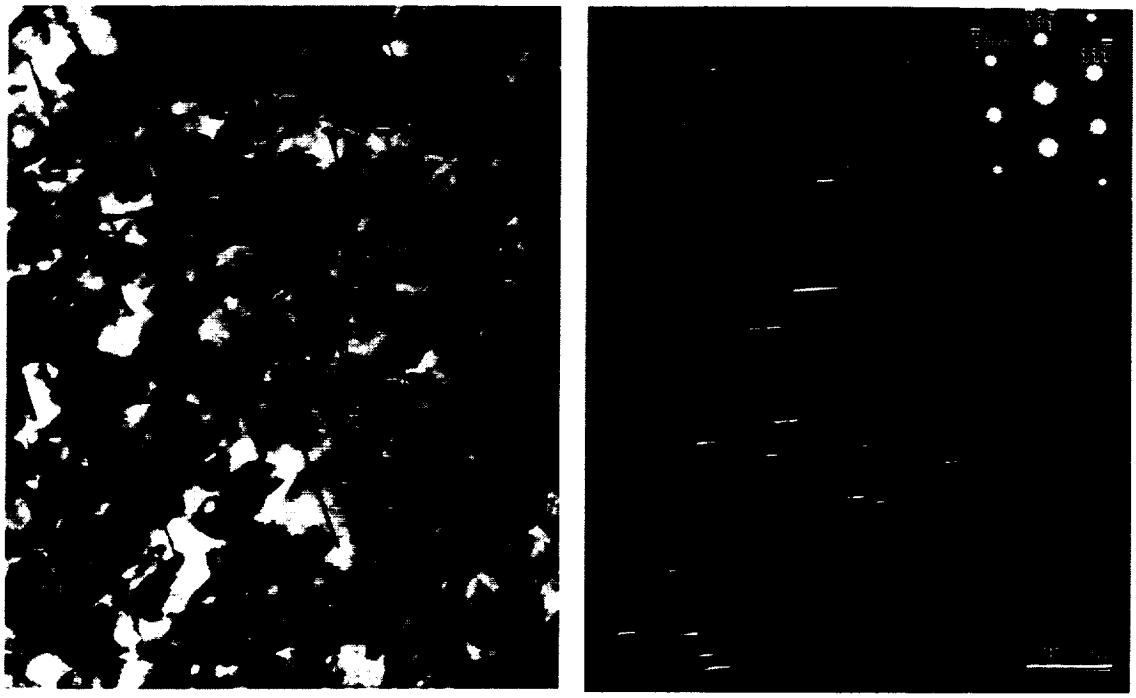

Bright Field Image Centered Dark Field Image

Figure 6 - Transmission electron micrographs representing the heat affected zone of alloy 2195-T8 at a position 12 mm from the fusion zone interface showing T_1 precipitates.

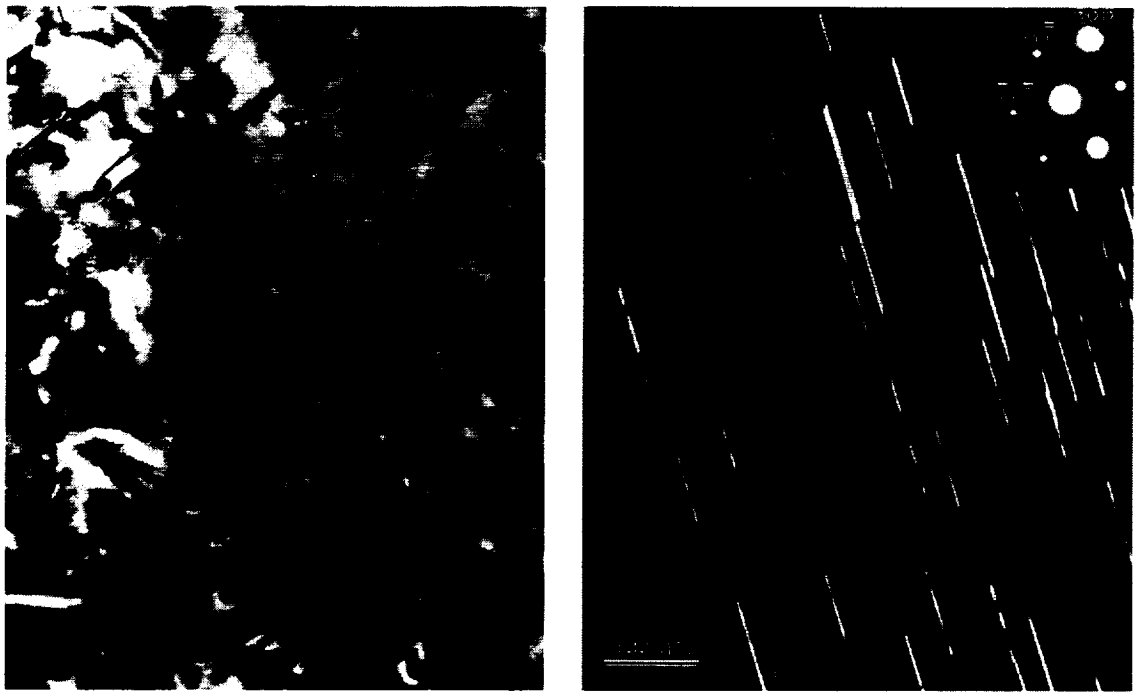

Bright Field Image Centered Dark Field Image

Figure 7 - Transmission electron micrographs representing the heat affected zone of alloy 2195-T8 at a position 7 mm from the fusion zone interface showing T_1 precipitates.

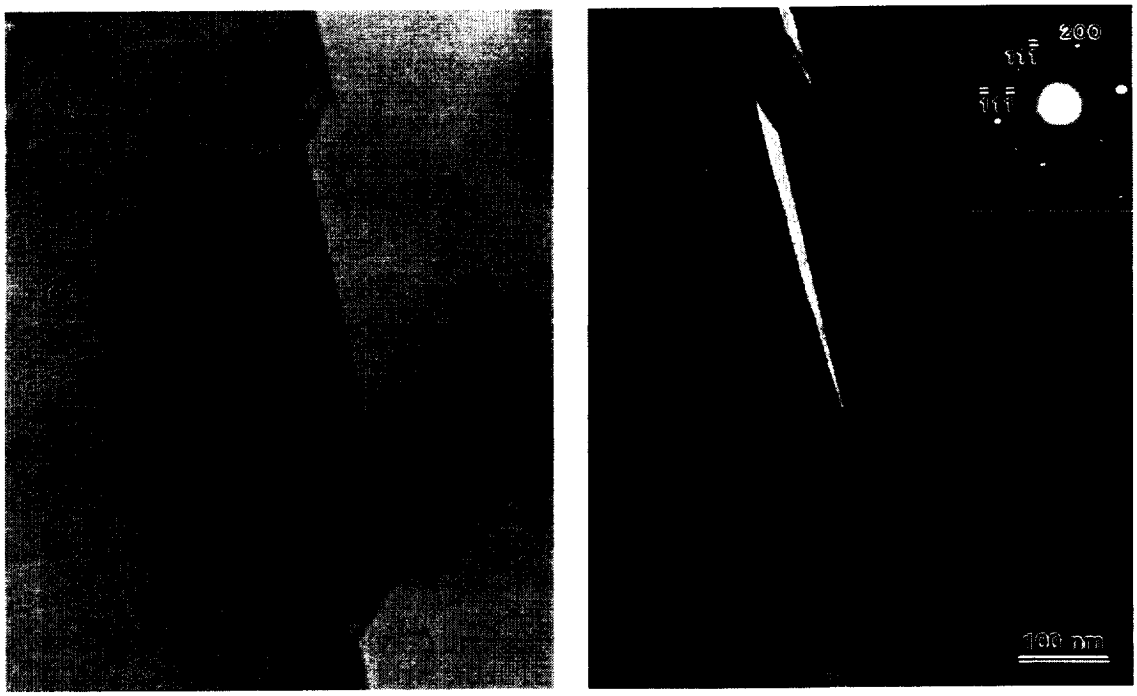

Bright Field Image **Centered Dark Field Image**

Figure 8 - Transmission electron micrographs representing the heat affected zone of alloy 2195-T8 at a position 1 mm from the fusion zone interface showing sub-boundary precipitation of T_1.

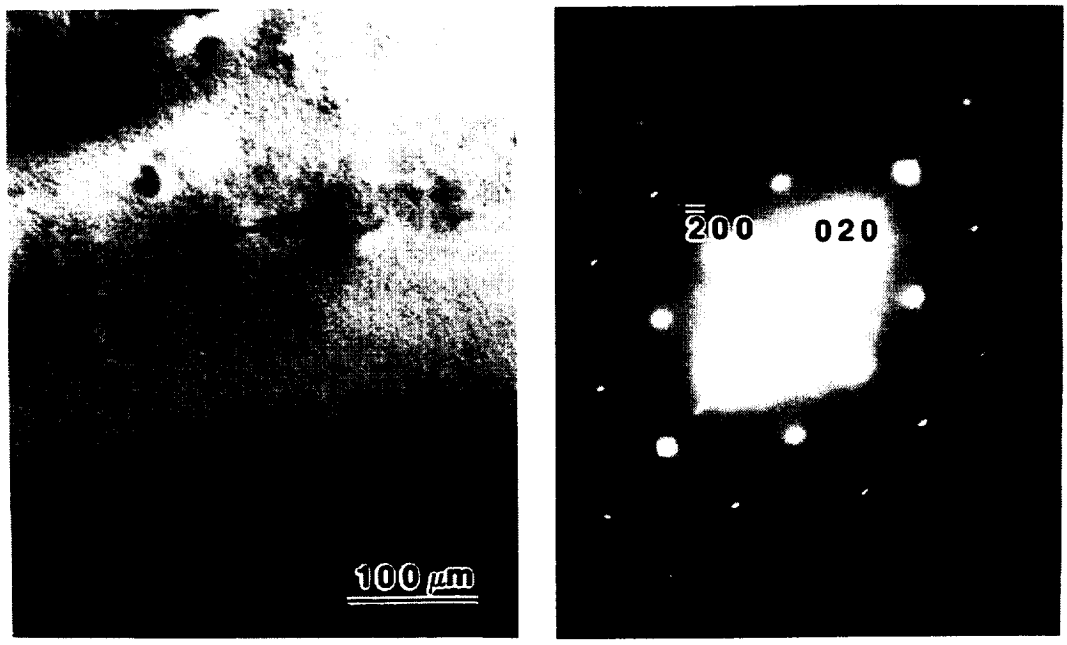

Figure 9 - Transmission electron micrograph and corresponding diffraction pattern representing the heat affected zone of alloy 2195-T8 at a position 1 mm from the fusion zone interface showing streaking along the <100> directions of the matrix which may indicate the presence of GP zones in this region.

2.2 Effects of Microstructural Modifications on Mechanical Properties

The effect of microstructure on strength within the various regions of the heat affected zone is governed by the ability to impede dislocation motion. The majority of the heat affected zone is governed by dislocation interaction with precipitates; although, a region adjacent to the fusion zone involves dislocation interaction with GP zones and the solid solution. If minor changes in grain size are considered negligible, the yield strength at various position within the heat affected zone may be represented as:

$$\sigma'_{ys} = \sigma_{ys} - 3\,(\Delta\tau_p - \Delta\tau_m) \qquad \text{Eq. 1}$$

where:

σ'_{ys} is the strength at a particular position in the heat affected zone,
σ_{ys} is the initial strength of the alloy in the peak-aged condition,
$\Delta\tau_p$ is loss in the critical resolved shear strength (CRSS) attributed to changes in precipitate size, spacing, and volume fraction, and
$\Delta\tau_m$ represents an increase in the CRSS due to solid solution strengthening of the matrix and is proportional to the concentration (C) of solute in solution as $C^{1/2}$.

The relationship between the CRSS and yield strength (Taylor Factor) has been shown to be close to the value of 3 for these alloys and is reflected in the right term of Equation 1 (Ref. 23&24).

Although the contribution of the precipitate and matrix to the CRSS may be considered linear (Ref. 25), strengthening contributions from dual precipitates (p_1 and p_2) have been shown to follow a generalized addition rule for Al-Cu-Li alloys (Ref. 24):

$$\Delta\tau_p^q = \Delta\tau_{p_1}^q + \Delta\tau_{p_2}^q \qquad \text{Eq. 2}$$

where q is an adjustable parameter with values between 1 and 2. The yield strength within the heat affected zones of Al-Cu-Li alloys may then be represented as:

$$\sigma'_{ys} = \sigma_{ys} + 3\Delta\tau_m - 3\left(\Delta\tau_{p_1}^q + \Delta\tau_{p_2}^q\right)^{1/q} \qquad \text{Eq. 3}$$

Huang and Ardell have shown that strengthening by T_1 plate precipitates could be estimated in terms of chemical strengthening or Orowan looping (Ref. 26). In either case, the variations in the CRSS could be correlated with changes in the volume fraction, thickness, and diameter of the T_1 plates. The most simplistic form, which described chemical strengthening by a strong particle, followed the relationship:

$$\Delta\tau_p = k\left(\frac{f}{\phi z}\right)^{1/2} \qquad \text{Eq. 4}$$

where:

$\Delta\tau_p$ is the contribution to the CRSS due to precipitate strengthening,
f is the volume fraction of precipitates,
ϕ is the average diameter of the plate precipitates,
z is the average width of the plates, and
k is a constant determined empirically and related to the interfacial energy between the precipitate and matrix.

In the case of Al-Cu-Li alloys, strength in the various regions of the heat affected zone is dependent upon the degree of dissolution during heating and re-precipitation upon cooling. At relatively low peak temperatures, partial dissolution results in loss of strength due to decreasing volume fraction of precipitates. Loss of precipitate strengthening is accompanied by minor increases in solid solution strengthening but the overall effect is a gradual decrease in strength as the fusion zone is approached. Heating to intermediate peak temperatures increases the degree of dissolution while increasing the amount of solute within the matrix. Larger precipitate that did not completely dissolve during heating provide the substrate for growth upon cooling from these temperatures. The volume fraction of precipitate increases, as well as solid solution strengthening.

Positions within the heat affected zone that experience high peak temperatures result in complete dissolution and re-precipitation upon cooling. Although solid solution strengthening of the matrix is operative, the major increase in strength is believed to be associated with re-precipitation of strengthening phases. In the case of alloy 2195-T8, the increase in strength associated with the region adjacent to the fusion zone may, at least, be attributed to the formation of GP zones. Increases in strength in this region with time after welding has been previously observed in laser beam welds of alloy 2195-T8 and may now be ascribed to the formation of Cu-rich zones (Ref. 6). It is worth noting that toughness for many of these alloys is influenced by microstructural features observed within a narrow region of the heat affected zone adjacent to the fusion zone interface. The presence of extensive grain boundary precipitates promotes intergranular fracture by the formation of micro-voids around grain boundary particles (Ref. 27), and coalescence of micro-voids within the PFZs (Ref. 28).

2.3 Summary of Microstructural Characterization

The base metal microstructure and evolution of microstructure within the heat affected zone Al-Cu-Li alloys have been discussed. Diffusion controlled modifications to strengthening precipitate in these systems have been qualitatively described in terms of solute concentrations at the interface and adjacent to the precipitate. It is observed that the ability to establish local equilibrium at the precipitate/matrix interface, which minimizes the chemical free energy of the system, will govern these structural modifications. Coarsening of precipitate is anticipated to be limited to positions experiencing relatively low temperatures; whereas, dissolution is expected to dominate the microsctructural modification within the heat affected zone for these alloys.

Transmission electron microscopy was performed on specimens removed from various regions of the heat affected zone of alloy 2195-T8. The base metal microstructure of this alloy in the peak aged temper was found to be dominated by T_1 (Al_2CuLi) and θ' (Al_2Cu) precipitates. Both of which form as plates on preferred planes of the matrix. Complete dissolution of θ' occurred within the heat affected zone at temperatures below 220°C (428°F), and partial dissolution of T_1 was observed for peak temperatures of 320°C (608°F). Moderate increases in the size of the T_1 precipitate was detected at peak temperatures approaching 500°C (932°F) and is believed to be caused by growth of partially dissolved precipitate during cooling.

The gradual loss of strength for positions representing these temperature regimes is believed to be attributed to dissolution of the T_1 precipitate. The relatively high peak temperatures associated with positions near the fusion zone interface resulted in complete dissolution of strengthening precipitate and re-precipitation of copper-rich zones upon cooling. The increased strength exhibited within this region is believed to be due to the formation of these zones and, to a lesser degree, solid solution strengthening. A narrow region of the heat affected zone that is adjacent to the fusion zone interface may influence weld toughness by the presence of precipitate free zones and solute depletion.

3.0 PARAMETRIC STUDY OF PROCESS PARAMETERS

A parametric study using a designed experiment methodology was performed to ascertain the effect of pretreatment, power, welding speed, defocusing, and the use of filler metal on porosity and fusion zone geometry. The objective of the task was to identify processing conditions that resulted in maximum width of the weld at the interface and minimal porosity. Processing parameters such as power, welding speed, and degree of beam defocusing, were evaluated. Chemical milling to remove 0.02 mm (0.001 in.) and 0.25 mm (0.010 in.) per side was assessed during the experiment, and the influence of autogenous welding and the use of filler metal additions on porosity was also ascertained. Fusion zone geometry was determined by metallographic techniques and radiographic analysis was used to distinguish weld porosity. Statistical analysis was employed to quantitatively determine the effects of processing conditions on weld attributes.

3.1 Factorial Experiment

A fractional factorial experiment was designed to measure the influence of process parameters on weld geometry and porosity (Ref. 29&30). The experiment entailed the evaluation of five variables (beam power, degree of defocus, travel speed, filler metal, and degree of chemical cleaning) at three levels for estimating the coefficients in a second degree, graduating polynomial. The fractional experiment was designed to efficiently establish the relationships between process parameters and important weld characteristics; however, the design allowed only first-order interactions of the independent variables to be established. Although a moderate decrease resolution is provided by this design it resulted in a substantial decrease in experimentation. The independent variables and levels that were utilized during the experiment are shown in Table 1. Prior to performing the experiment, evaluations were conducted to establish a process parameter envelope that would provide between 30 and 70 percent weld penetration into the thicker member (skin-sheet) of the lap-weld. Based on these results, the levels of the independent variables were established for the experiment.

Material requiring pretreatment was chemically milled in a NaOH aqueous solution by Chem-Tronics Corporation, El Cajon, CA. Chem-Tronics Corporation was chosen to perform the chemical milling based on their past program performance. Although exact chemical milling parameters were considered proprietary by Chem-Tronics, it was specified that material could not exceed 104°C (220°F) for more than 10 minutes during milling. Samples were individually wrapped and returned to the ARL Penn State by over-night carrier after chemical milling. The various thicknesses of material provided by NASA Langley Research Center was utilized to obtain constant material thicknesses of the stiffener and skin components. Therefore, all lap-welds were produced on 0.50 in. 1.25 mm (0.050 in.) thick 2195-T6 welded to 3.12 mm (0.125 in.) thick 2195-T8. Lap-welds were produced on specimens 84 mm (3.3 in.) wide and 254 mm (10.0 in.) in length that were fully overlapped. Welds were produced along the length and were parallel to the rolling direction. Automated welding of the specimens was performed using the Laser Articulating Robotic System (LARS) and a 14 kW United Technologies CO_2 laser. Uniform clamping was achieved through the use of a weld fixture providing clamping force at three point along each side of the specimens. The optical arrangement used on LARS in shown in Figure 10.

Table 1
Variables and Levels That Were Utilized in Fractional Factorial Experiment

Variables	Level	Description
1: Laser Power	-1	8.0 kW
	0	10.0 kW
	+1	12.0 kW
2: Travel Speed	-1	8.5 cm/s (200 IPM)
	0	10.6 cm/s (250 IPM)
	+1	12.7 cm/s (300 IPM)
3: Beam Defocus	-1	At Focus: 12.7 cm (5.00 in.) Stand-off
	0	Below Focus1: 13.3 cm (5.25 in.) Stand-off
	+1	Below Focus2: 14.0 cm (5.50 in.) Stand-off
4: Filler Metal	-1	Without Filler Metal
	0	Filler1: 1.2 mm (0.046 in.) Diameter Alloy 2319 at 2.1 cm/s (50 IPM) Feed Rate
	+1	Filler2: 1.2 mm (0.046 in.) Diameter Alloy 2319 at 4.2 cm/s (100 IPM) Feed Rate
5: Pretreatment	-1	As-Received Material
	0	Chemically Milled to Remove 0.02 (0.001 in.)
	+1	Chemically Milled to Remove 0.25 mm (0.010 in.)

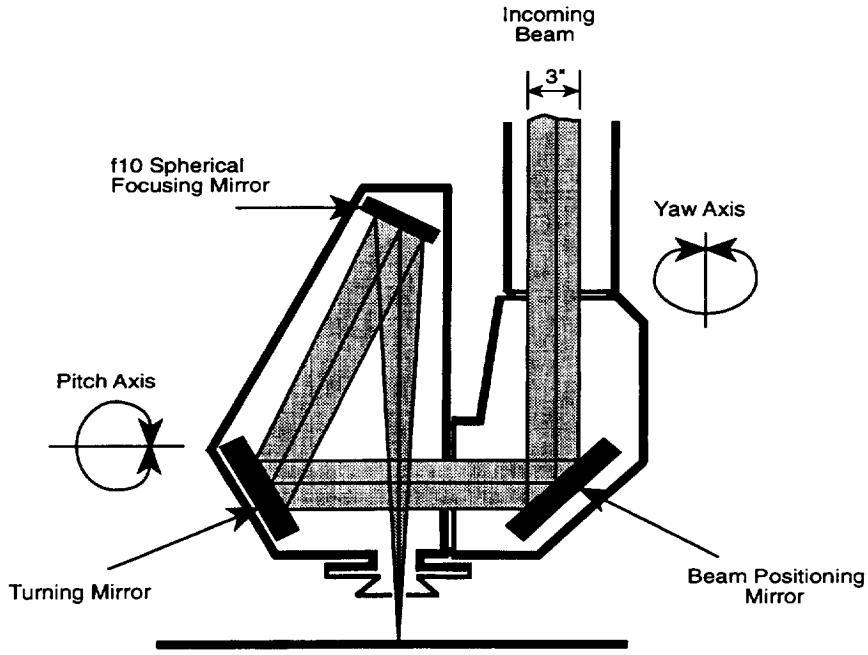

Figure 10 - Optical Arrangement of Laser Articulating Robotic System Used to Perform the Parametric Study.

The total number of experimental runs conducted during the study were 46, with 6 runs being replications of the parametric center. The experiments were blocked by the variable stand-off distance and randomized within these blocks. After welding, specimens were visually inspected and sectioned for metallographic and radiographic preparation. Visual inspection was performed by four individuals using criteria based on positive weld-bead reinforcement and process stability. Specimens were ranked on a scale of 1 to 10, 10 exhibiting an excellent appearance. The rankings of visual inspection of the four individuals were then averaged. After visual inspection, the weld panels were sectioned at the mid-length of the weld. Metallographic samples were removed for measuring weld penetration and width at the interface between the top-sheet and skin-sheet. The other half of the specimens, representing approximately 10.2 cm (4 in.) of weld, were radiographed using a 50 kV accelerating voltage and 2.8 mA current. A five-film porosity standard having rankings of 1.0 to 5.0 was constructed using radiographs from five welds. The experimental runs representing the radiographs used for the standard were: run 40 representing a ranking of 1.0, run 14 representing a ranking of 2.0, run 18 representing a ranking of 3.0, run 12 representing a ranking of 4.0, and run 37 representing a ranking of 5.0. Although some porosity was evident in all radiographs, a ranking of 1.0 representing minimum porosity within the weld. This standard was employed to rank the radiographs based on porosity by three individuals. The rankings of the three individuals were then averaged.. The five-film porosity standard used to rank the radiographs of all welds is shown in Figure 11. Results of the visual inspection, metallographic analyses, and radiographic inspection are shown, along with process parameters used for the fractional factorial experiment, in Table 2. Note, in some cases measurements of the dependent variable could not be performed due to lack of coupling, lack of penetration into the skin-sheet, etc.

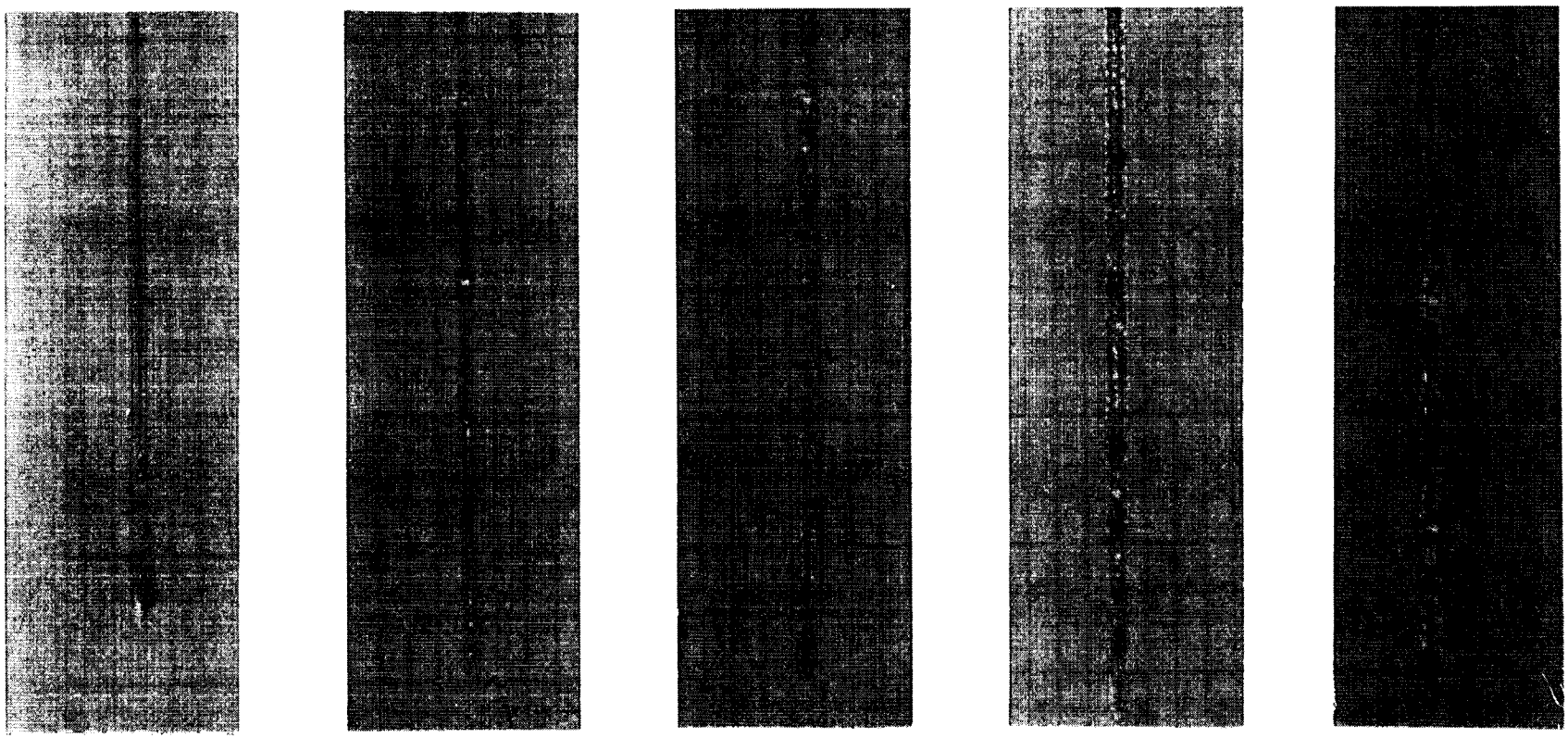

Figure 11 - Five-Film Porosity Standard Used to Rank Radiographs of Welds Produced During Parametric Study.

Table 2
Process Parameters and Results of Fractional Factorial Experiment

Run	Power (kW)	Speed (cm/s)	Stand-off (cm)	Removal (mm)	Filler (cm/s)	Visual Rating	Interface (mm)	Depth (mm)	Porosity Rating
1	12	12.7	13.3	0.02	2.1	6.2	1.8	2.8	3.5
2	12	8.5	13.3	0.02	2.1	6.2	1.4	5.1	3.1
3	8	12.7	13.3	0.02	2.1	*	*	*	*
4	8	8.5	13.3	0.02	2.1	*	*	*	*
5	10	10.6	14.0	0.02	4.2	6.4	1.6	2.2	3.2
6	10	10.6	14.0	0.02	0	4.6	1.7	2	2.6
7	10	10.6	12.7	0.02	4.2	7.8	1.0	4.6	2.1
8	10	10.6	12.7	0.02	0	6.0	1.2	3.6	2.9
9	10	12.7	13.3	0.25	2.1	5.6	1.0	2.0	1.0
10	10	12.7	13.3	0.0	2.1	4.0	1.9	3.0	4.3
11	10	8.5	13.3	0.25	2.1	5.2	1.4	3.8	3.4
12	10	8.5	13.3	0.0	2.1	4.4	1.6	5.2	*
13	12	10.6	14.0	0.02	2.1	6.4	2.0	2.5	2.0
14	12	10.6	12.7	0.02	2.1	7.6	1.4	4.6	*
15	8	10.6	14.0	0.02	2.1	*	*	*	*
16	8	10.6	12.7	0.02	2.1	2.8	0.9	2.4	3.5
17	10	10.6	14.0	0.25	4.2	5.4	1.9	2.6	2.3
18	10	10.6	14.0	0.0	4.2	4.4	1.6	3.2	*
19	10	10.6	12.7	0.25	0	2.8	1.3	3.1	2.7
20	10	10.6	12.7	0.0	0	3.4	1.5	3.2	2.9
21	10	10.6	13.3	0.02	2.1	2.0	1.2	3.3	2.0
22	10	10.6	13.3	0.02	2.1	4.2	1.1	3.2	1.9
23	10	10.6	13.3	0.02	2.1	6.4	1.9	3.7	3.1
24	10	12.7	14.0	0.02	2.1	1.2	*	1.1	*
25	10	12.7	12.7	0.02	2.1	6.0	1.4	2.8	1.3
26	10	8.5	14.0	0.02	2.1	5.6	1.9	2.8	3.9
27	10	8.5	12.7	0.02	2.1	6.6	1.4	4.2	2.4
28	12	10.6	13.3	0.02	4.2	6.6	1.2	4.8	2.5
29	12	10.6	13.3	0.02	0	6.4	1.6	3.7	2.0
30	8	10.6	13.3	0.02	4.2	*	*	*	*
31	8	10.6	13.3	0.02	0	*	1.7	5	*
32	10	10.6	14.0	0.25	2.1	4.2	1.9	2.4	1.0
33	10	10.6	14.0	0.0	2.1	4.2	2.3	3.7	4.0
34	10	10.6	12.7	0.25	2.1	6.6	1.1	3.8	2.4
35	10	10.6	12.7	0.0	2.1	4.8	1.8	5.3	4.8
36	12	10.6	13.3	0.25	2.1	4.8	1.5	3.8	1.8
37	12	10.6	13.3	0.0	2.1	3.8	*	1.6	*
38	8	10.6	13.3	0.25	2.1	3.2	1.1	2	1.0
39	8	10.6	13.3	0.0	2.1	3.6	1.6	2.4	1.0
40	10	12.7	13.3	0.02	4.2	5.4	1.3	2.7	*
41	10	12.7	13.3	0.02	0	6.4	1.0	1.8	1.0
42	10	8.5	13.3	0.02	4.2	6.8	1.5	5	4.1
43	10	8.5	13.3	0.02	0	6.8	1.4	4.1	3.3
44	10	10.6	13.3	0.02	2.1	5.4	1.3	3.8	2.2
45	10	10.6	13.3	0.02	2.1	4.0	1.2	3.2	3.4
46	10	10.6	13.3	0.02	2.1	6.4	1.3	3.4	2.0

* Measurements of the dependent variable could not be performed due to lack of coupling, lack of penetration into the skin-sheet, etc.

Results of the fractional factorial experiment were analyzed using multiple regression analyses employing a least-squares fit at a 90% confidence interval. Initial analyses entailed the identification of process parameters having a significant influence on the dependent variables of visual ranking, weld penetration, weld width at the interface, and porosity ranking. The criteria utilized to identify significant parameters was based on a 90% probability level of rejecting the null hypothesis. The significant process parameters identified during multiple regression analyses are summarized for each dependent variable in Table 3.

Table 3
Summary of Initial Multiple Regression Analyses Showing Independent Variables Having a Significant Effect on the Dependent Variables

Dependent Variable	Independent Variable	Coefficient	t-Value	Probability
Visual Ranking	Power	+0.636	2.971	0.0053
	Stand-off (Defocus)	-0.891	1.742	0.0903
Penetration	Velocity	-0.473	4.905	0.0001
	Stand-off (Defocus)	-1.100	3.868	0.0004
Width at Interface	Stand-off (Defocus)	+0.442	4.172	0.0002
Porosity Ranking	Pretreatment	-3.724	2.236	0.0332
	Velocity	-0.267	1.931	0.0633

The sign of the coefficient from the fitted linear relationships provided an indication of the influence of the individual process parameters (independent variables) on the weld characteristics of interest (dependent variables). Higher visual rankings could be attributed to higher power and greater stand-off distance (greater degree-of-defocus). Weld penetration was decreased by higher welding velocities and greater stand-off. Although a significant relationship between welding power and weld depth was anticipated, the lack-of-penetration into the skin sheet during welding at 8.0 kW precluded depth data from these welds and probably negated the ability to provide a statistical significance between power and weld depth. The width of the weld at the interface position was found to be strongly effected by the stand-off distance (degree-of-defocus). As expected, weld width increased as stand-off increased. Weld porosity, based on the results of radiographic rankings, increased as welding velocity decreased and amount of chemical milling decreased.

Additional analyses was performed on penetration, width, and porosity. These attributes were considered the primary dependent variables of interest. Regression analyses was conducted utilizing only the independent variables having significant effect on these response variables, which are shown in Table 3. The results of these analyses continued to indicate the influence of the independent variables shown to have statistical significance during the initial analyses; however, a reduction in the number of the independent variables allowed fitted relationships to be developed based on one or two variables. The relationships obtained from the least-squares fit, which indicate the effect of primary process parameters on critical weld attributes, are shown below:

$$\text{Radiographic Rating} = 5.701 - 3.756\,(P) - 0.270\,(V) \qquad \text{Eq. 5}$$

$$\text{Interface Width (mm)} = -4.198 + 0.426\,(S) \qquad \text{Eq. 6}$$

$$\text{Weld Depth (mm)} = 21.341 - 0.473\,(V) - 0.977\,(S) \qquad \text{Eq. 7}$$

where in the above relationships: P is amount removed during pretreatment in mm, V is welding velocity in cm/s, and S is stand-off distance in cm (stand-off represents degree-of defocus). The fitted data for these relationships are also shown graphically in Figures 12 through 14. Figure 12 illustrates the statistical relationship of penetration as a function of welding velocity and stand-off, or degree of defocus. The bound area represents penetration required to achieve between 40 and 60 percent into the skin-sheet (3.1 to 3.8 mm). Figure 13 shows the relationship of weld width at the interface based on stand-off. It is apparent that a wider weld interface may be achieved with greater stand-off, or a greater degree of defocus. Figure 14 represents the relationship for porosity ranking as a function of welding velocity and amount of removal per side by chemical milling prior to welding. The figure graphically illustrates that weld porosity is minimized by aggressive pretreatment and high welding velocity. Higher welding velocity is believed to decrease porosity by decreasing the amount of penetration into the skin-sheet; however, adequate weld quality requires a minimum amount of penetration (which has been selected as representing between 40 and 60 percent into the skin sheet.

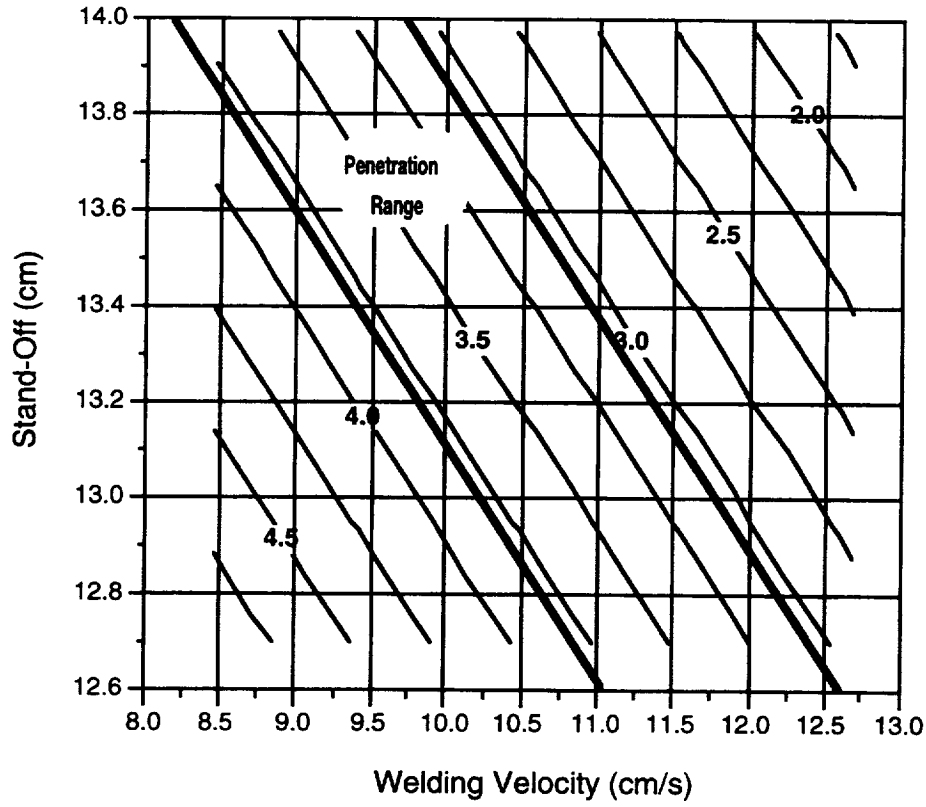

Figure 12 -Statistical Relationship Showing Isolines for Penetration in mm as a Function of Welding Velocity and Stand-off (bound area represents penetration required to achieve between 40 and 60 percent into the skin-sheet).

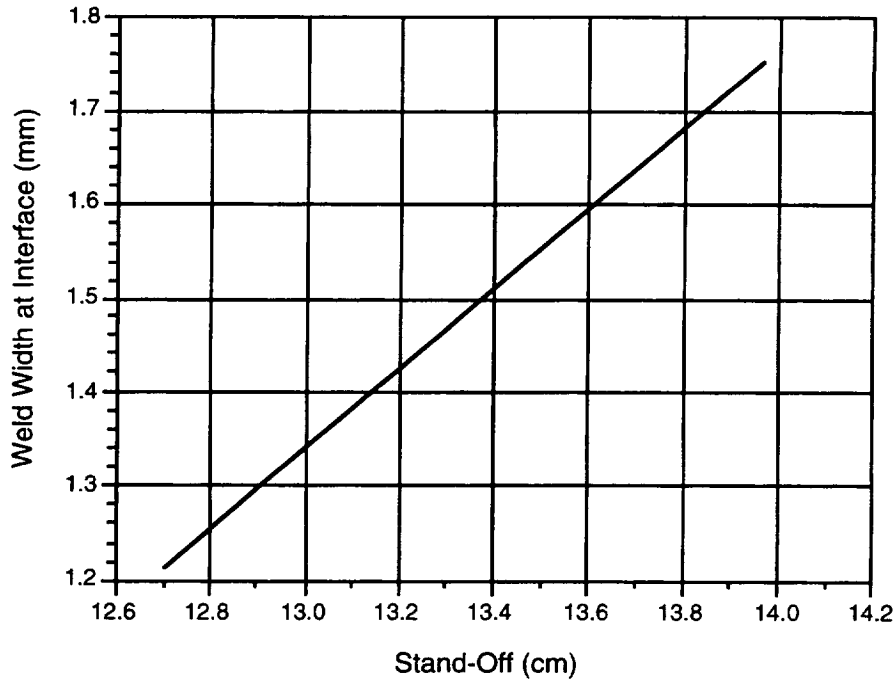

Figure 13 -Statistical Relationship Showing Width of Weld at Interface as a Function of Stand-off (or degree of defocus).

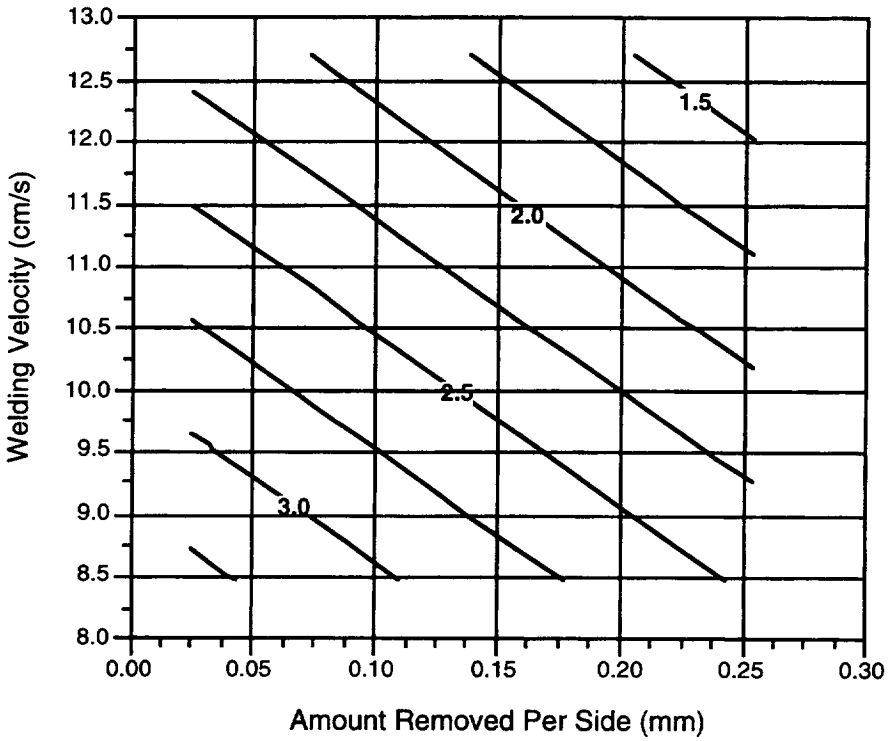

Figure 14 -Statistical Relationship Showing Isolines for Porosity Ranking as a Function of Amount Removed Per Side by Chemical Milling Prior to Welding and Welding Velocity.

Based on the statistically derived relationships, values for critical process parameters that provided an optimal weld profile while minimizing porosity were identified. These parameters were: 13.3 cm (5.25 in.) stand-off to maximize weld width at the interface while providing adequate penetration into the skin-sheet, a welding velocity of 10.6 cm/s (250 IPM) to minimize porosity while also providing adequate penetration, and chemical milling of 0.25 mm (0.010 in.) per side prior to welding to minimize susceptibility to weld porosity. As discussed earlier, statistical relationships for laser power could not be developed from results of the factorial experiment, therefore, a confirmation evaluation was conducted to optimal identify laser welding power at the defined stand-off and pretreatment conditions.

Confirmation specimens were produced with alloy 2195 using optimal parameters identified from results of the parametric study. The confirmation evaluation included the use of three laser powers in conjunction with the previously identified parameters. The powers utilized during welding of these specimens were 9, 10, and 11 kW. Laser beam lap-welds were produced on specimens 8.4 cm (3.3 in.) wide and 25.4 cm (10.0 in.) in length that were fully overlapped. Welds were produced along the length and were parallel to the rolling direction. Material utilized for welding had been chemically milled in an aqueous NaOH solution to remove 0.25 mm (0.010 in.) per side. This resulted in lap welds being produced on 1.27 mm (0.050 in.) thick 2195-T6 to 3.12 mm (0.125 in.) thick 2195-T8. Prior to welding, all material was solvent cleaned with acetone. As with the earlier experiment, automated welding of the specimens was performed using the Laser Articulating Robotic System and a 14 kW United Technologies CO_2 laser. Uniform clamping was achieved through the use of a weld fixture providing clamping force at three points along each side of the specimens.

Weld specimens representing the three powers were inspected by radiography and optical microscopy. The specimens were sectioned at the midpoint along the weld length. One side was used for metallographic samples and the other side was radiographed. Samples, representing approximately 4.0 in. (10.2 cm) of weld, were radiographed using positive film with an accelerating voltage of 50 kV, a current of 2.8 mA, and a 150 second exposure time.

Photographic copies of the radiographs representing the three welds produced at 9, 10, and 11 kW of power are shown in Figure 15. Macrographs representing the cross-sections of these welds are also shown in Figure 16. The radiographs indicated that very little porosity was present within the welds produced at 9 and 10 kW; whereas, the weld produced at 11 kW exhibited considerable fine porosity having a diameter less than 0.25 mm (0.010 in.). The location of porosity within the weld produced using 11 kW of power is near the weld edge, and was possibly associated with the corner of the interface between the two sheets. The macrographs of Figure 16 indicate marginal penetration at 9 kW of power and adequate penetration associated with the welds produced at 10 or 11 kW of output power. Fine porosity along the weld root was also displayed in the macrograph of the weld produced at 10 kW.

3.2 Summary of Parametric Study

A three-level fractional factorial experiment was conducted to establish quantitative relationships between primary process parameters and critical weld attributes. The experiment entailed the evaluation of five independent variables (beam power, degree of defocus, travel speed, filler metal, and degree of chemical cleaning) at three levels. The dependent response variables for the evaluation included the width and depth of penetration and radiographic rating for weld soundness. Strong statistical correlation was observed for : weld penetration as a function of welding velocity and stand-off distance, weld width at the interface as a function of stand-off distance, and porosity rating as a function of amount removed by chemical milling and welding velocity. Although a significant relationship between welding power and weld depth was anticipated, the lack-of-penetration into the skin sheet during welding at the lowest power precluded data from these welds

and negated the ability to provide a statistical significance between power and weld geometry. Therefore, a confirmation experiment, having improved resolution for process power, was conducted identify optimal process parameters. Parameters were identified for maximizing weld width while maintaining adequate penetration and minimizing porosity. Results of these experiments yielded optimal process parameters for welding of stiffeners to skin. These parameters were: an output power of 10 kW, a processing speed of 10.6 cm/s (250 IPM), a stand-off distance of 13.3 cm (5.25 in.), and chemical milling of 0.25 mm (0.010 in.) per side prior to welding.

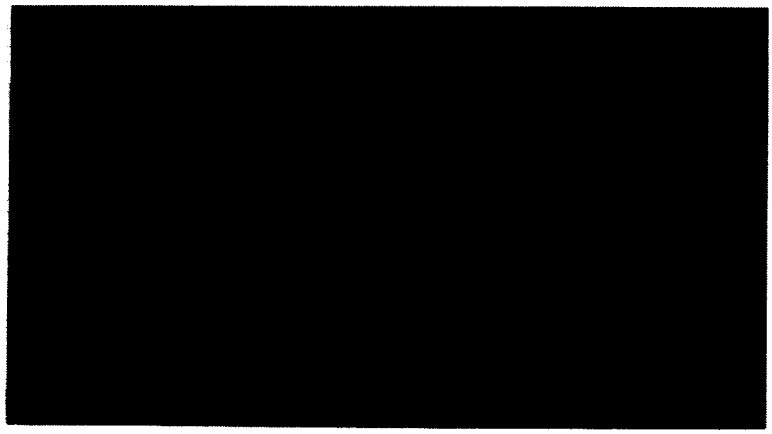

(a) Weld Produced at 9 kW, 13.3 cm Stand-Off, and 10.6 cm/s

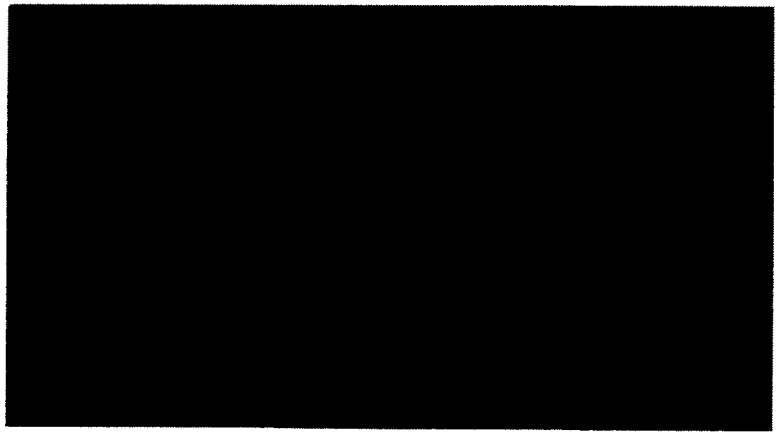

(b) Weld Produced at 10 kW, 13.3 cm Stand-Off, and 10.6 cm/s

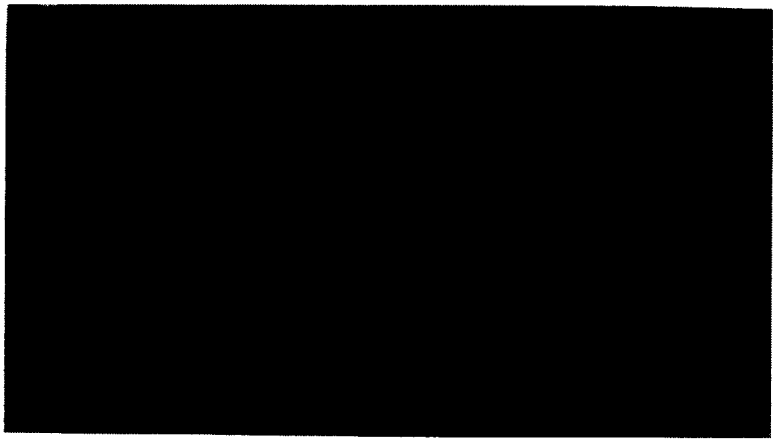

(c) Weld Produced at 11 kW, 13.3 cm Stand-Off, and 10.6 cm/s

Figure 15 - Photographic Copies of Radiographs of Welds Produced During the Experiment to Confirm Welding Process Parameters.

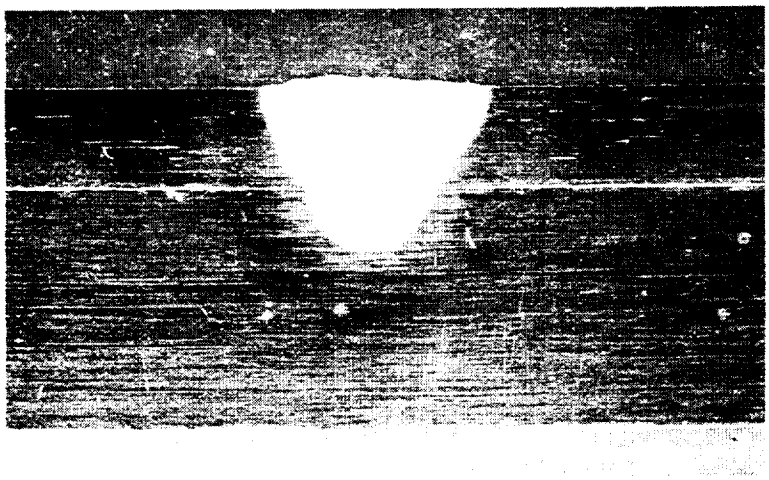

(a) Weld Produced at 9 kW, 13.3 cm Stand-Off, and 10.6 cm/s

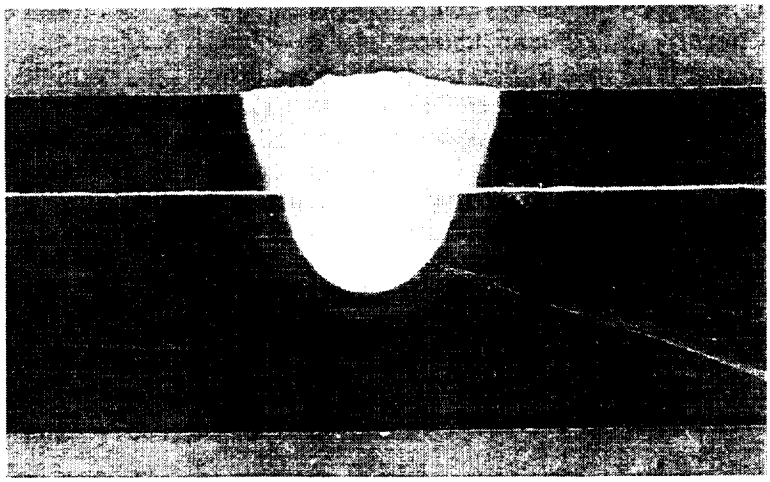

(b) Weld Produced at 10 kW, 13.3 cm Stand-Off, and 10.6 cm/s

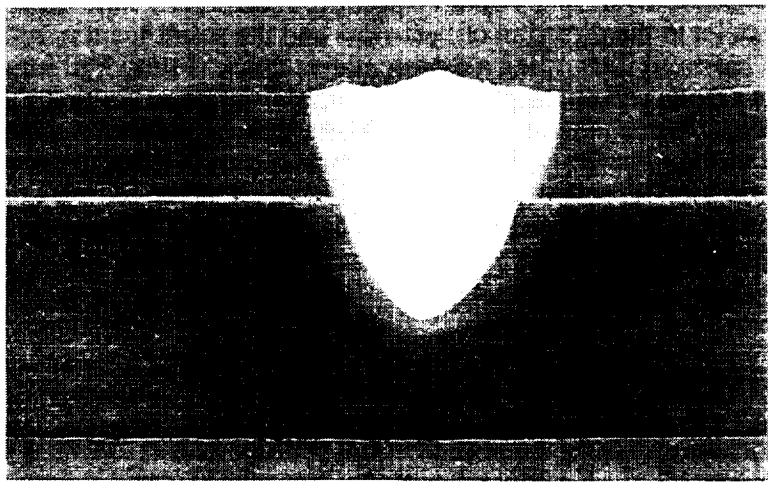

(c) Weld Produced at 11 kW, 13.3 cm Stand-Off, and 10.6 cm/s

Figure 16 - Macrographs of Welds Produced During the Experiment to Confirm Welding Process Parameters.

4.0 REPRODUCIBILITY STUDY

A reproducibility study using optimal parameters was conducted to establish expected consistency during laser beam welding. The objective of this task was to produce a minimum of 305 cm (10 ft.) of weld for testing.

4.1 Reproducibility Experiment

A reproducibility experiment was initiated to assess process consistency. Laser beam lap-welds on 2195 were produced at 11.0 kW of power, 10.6 cm/s (250 IPM) travel speed, and a stand-off distance between the focus head and part of 13.3 cm (5.25 in.). The 11.0 kW of output power resulted in 8.5 kW of actual power, measured by a calorimeter, to the work-piece. The stand-off distance resulted in defocusing of the beam approximately 6.35 mm (0.25 in.) above the part. All material was chemically milled in an aqueous NaOH solution at Chem-tronics Corporation, El Cajon, Ca. to remove 0.25 mm (0.010 in.) prior to welding. This resulted in lap welds being produced on 1.27 mm (0.050 in.) thick 2195-T6 to 3.12 mm (0.125 in.) thick 2195-T8. Prior to welding, all material was solvent cleaned with acetone. Automated welding of the specimens was performed using the Laser Articulating Robotic System and a 14 kW United Technologies CO_2 laser. Uniform clamping was achieved through the use of a weld fixture providing clamping force at three points along each side of the specimens.

Laser beam lap-welds were produced on specimens 15.2 cm (6.0 in.) wide and 30.5 cm (12.0 in.) in length with a 10.2 cm (4.0 in) overlap. This sample geometry was chosen such that sub-size tensile specimens of the partial penetration weld of the skin sheet and tension shear specimen of the stiffener-to-skin could be obtained from the same panel configuration. Welds were produced along the length and were parallel to the rolling direction.

Visual inspection at 20X magnification was performed after approximately 122 cm (4 ft.) of weld was produced. Although weld consistency appeared high, numerous cracks on the top-surface of the welds were discovered during visual inspection. The cracks were transverse to the welding direction and parallel to the direction of heat-flow and the solidification front. A photograph of the top-surface of a lap-weld illustrating a representative crack is shown in Figure 17. To determine the possibility of cracks present in prior welds, samples produced during the parametric experiment were also inspected. Upon examination at 20 X magnification, cracks were also found on the top-surface of these welds. The crack direction and appearance of these cracks were identical to the cracks found during the reproducibility study. The cracks in the samples produced during the parametric experiment were not detected by radiography. Based on the results of visual inspection, the reproducibility study was terminated until methods to eliminated weld cracking could be identified.

4.2 Summary of Reproducibility Study

A reproducibility study using optimal parameters was conducted to assess process consistency during laser beam welding. The objective of this task was to produce a minimum of 305 cm (10 ft.) of weld for testing. Although weld consistency appeared high, numerous cracks on the top-surface of the welds were discovered during visual inspection after approximately 122 cm (4 ft.) of weld was produced. The cracks were transverse to the welding direction and parallel to the

direction of heat-flow and the solidification front. Based on the results of visual inspection, the reproducibility study was terminated until methods to eliminated weld cracking could be identified.

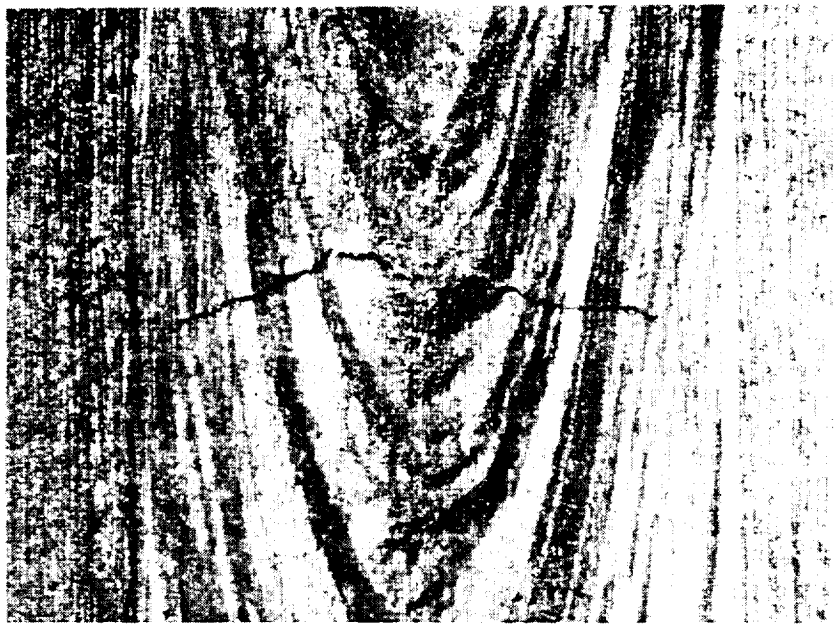

Figure 17 - Photograph of Top Surface of Weld From Panel Produced During Reproducibility Study Showing Representative Crack in Weld (Photograph at approximately 20X magnification).

5.0 WELD CRACKING INVESTIGATION

The results of visual inspection indicated the presence of transverse cracks at the top surface of the lap welds produced during the reproducibility study. The cracks were believed to form during solidification of the weld pool which represented the base metal composition of alloy 2195 since all welds of the reproducibility study were produced autogenously. The propensity for solidification cracking of aluminum alloys during welding is highly sensitive to the composition of the weld. Therefore, obvious methods for negating weld cracking would be the alteration of weld pool chemistry by filler alloy additions.

The original task description for the program was modified to include an evaluation of various filler alloys on the weld crack sensitivity during laser beam welding of alloy 2195. The objective of this task was to identify a filler alloy and process parameters that could eliminate solidification cracking. The selection of process parameters would ultimately rely on the ability to maximize the filler alloy dilution during welding. An initial experiment was conducted to screen various filler alloys and a subsequent evaluation was performed to maximize filler metal dilution through modification of the established process parameters.

5.1 Initial Filler Alloy Experiment

An initial experiment was conducted to identify filler alloys showing promise for eliminating solidification cracks. The parameters and specimen configuration utilized during this experiment were identical to those used during the reproducibility study; however, filler alloy additions were made by feeding filler wire into the rear of the solidifying weld pool. Filler alloys that were evaluated included: alloy 2319 (Al-6.3 Cu), alloy 4043 (Al-5.3 Si), alloy 4047 (Al-12Si), alloy 4145 (Al-10Si-4Cu), and alloy 5356 (Al-5.0Mg). Autogenous welds were also produced for comparison purposes.

The effect of various filler alloys on crack sensitivity was ascertained by quantitatively determining the amount of cracking associated with each laser beam weld produced at constant welding parameters but with various filler alloys. Autogenous welds were also produced for comparison purposes. All lap welds were produced at a power 11.0 kW (8.5 kW to the work-piece), 10.6 cm/s (250 IPM) travel speed, stand-off distance of 13.3 cm (5.25 in.), and a wire feed rate of 6.6 cm/s (125 IPM) for the 1.2 mm (0.046 in.) diameter filler wire. Material was chemically milled 0.25 mm (0.010 in.) per side prior to welding. Two panels were produced for each filler alloy. To quantitatively determine crack sensitivity, welds were visually inspected at approximately 10X magnification and the total crack length for all cracks along the weld were summated and recorded. This data was then normalized by dividing the total crack length by the total length the welds examined. Metallographic analyses was also conducted on welds to determine the depth and orientation of the cracks and atomic absorption was used to determine compositions associated with the weld fusion zones.

The results of the filler alloy evaluation in terms of average total crack length per weld length is shown in Figure 18. As illustrated in the figure, filler alloys having high levels of silicon may be used to reduce solidification cracking. Shown in Table 4 are chemical compositions of the fusion zones, obtained by atomic absorption, for welds produced during the filler alloy evaluation. The nominal composition of 2195 base metal is also shown in Table 4. The dilution of filler metal to base metal may be calculated from this data and was estimated to be less than 10 percent filler metal. Although weld metal composition was not significantly altered by filler alloy additions, modest increases in silicon resulted in a marked reduction in weld cracking. Based on these results, process modifications would be evaluated for increasing filler metal dilution.

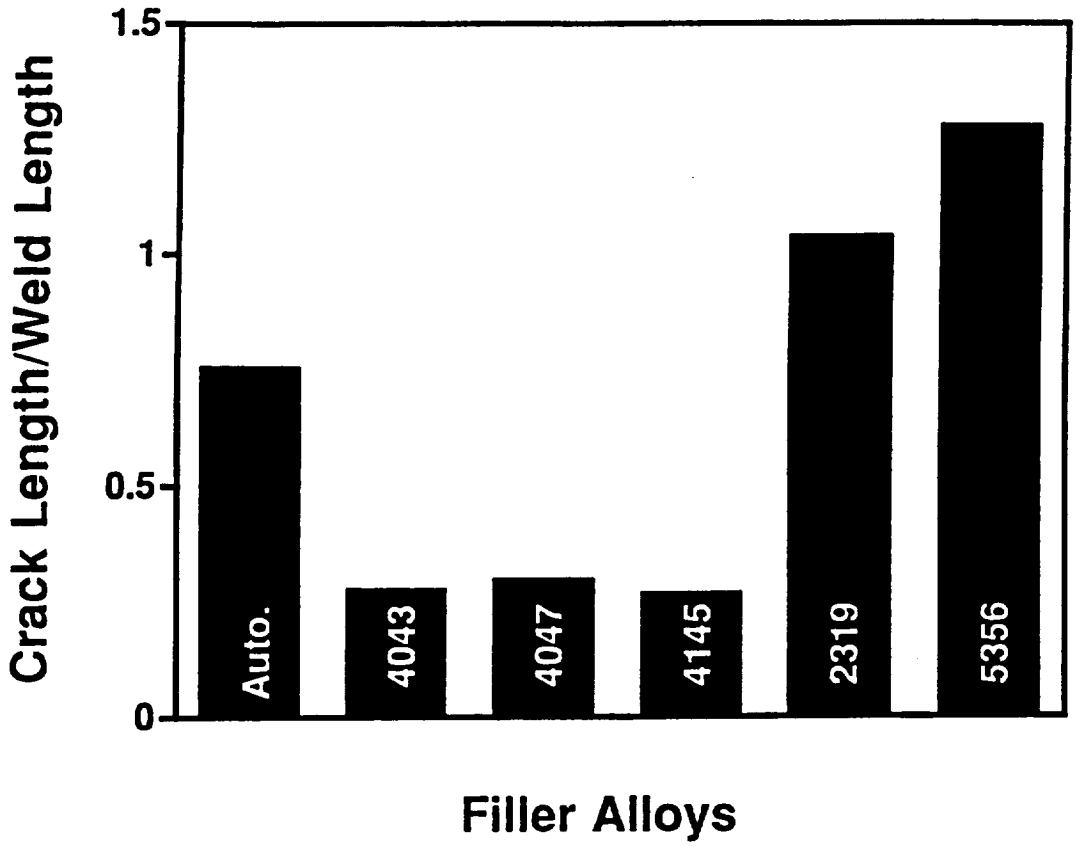

Figure 18 - Results of the Filler Alloy Evaluation in Terms of Average Total Crack Per Weld Length.

Table 4
Composition of Weld Fusion Zones, in Weight Percent, for Laser Beam Welds of 2195 Produced with Various Filler Alloys

Filler Alloy	Cu	Li	Mg	Si
2195 Base Metal[1]	4.00	1.00	0.40	-
Autogenous Weld	3.93	0.82	0.13	0.04
4043 Weld	3.47	0.90	0.17	0.39
4047 Weld	3.44	0.80	0.12	1.02
4145 Weld	3.85	0.81	0.12	0.59
2319 Weld	4.12	0.78	0.11	0.06
5356 Weld	3.65	0.85	0.25	0.05

[1] Composition of 2195 is shown as nominal and includes 0.40 Ag and 0.12 Zr.

5.2 Analyses of Weld Cracks

Metallographic and thermal analyses was performed to better understand the mechanism governing weld cracking during laser beam welding of alloy 2195. The ARC3.0 welding heat transfer program was used to simulate isotherms developed during laser beam welding. Although the ARC3.0 program was constructed to simulate heat input from a moving heat source through conduction of heat from the top surface, it may be used to approximate heat transfer conditions associated with laser beam welds having shallow vapor cavities. The photograph of Figure 17 shows a typical crack orientation at the top-surface of the laser beam welds. Figure 19 is simulative isotherms obtained from the ARC3.0 program and representative of the weld shown in Figure 17.

Metallographic specimens were prepared from samples removed longitudinally from the weld centerline near the top-surface of the welds produced autogenously and with 2319 and 4047 filler alloy. Specimens were prepared using normal metallographic techniques and etched with Keller's Reagent. Micrographs obtained from these welds are shown in Figure 20 at 100X and 500X magnification. Analysis of these specimens indicated multiple cracks having average depths of 1.45 mm (0.057 in.) for the autogenous weld, 1.22 mm (0.048 in.) for the weld produced with 2319, and 1.48 mm (0.058 in.) for the weld produced with 4047.

Optical metallography in conjunction with simulative thermal cycles was used to construct a composite schematic of solidification cracking of 2195 during laser beam welding, which is shown in Figure 21. As illustrated, cracks are initiated during solidification within the two-phase region near the rear of the liquid pool. This area is represented as an equiaxed region near the center of the weld and includes the presence of intergranular liquid, yet to solidify. Propagation of the cracks are in the direction of heat flow and along columnar-dendritic boundaries in an area adjacent to the equiaxe region.

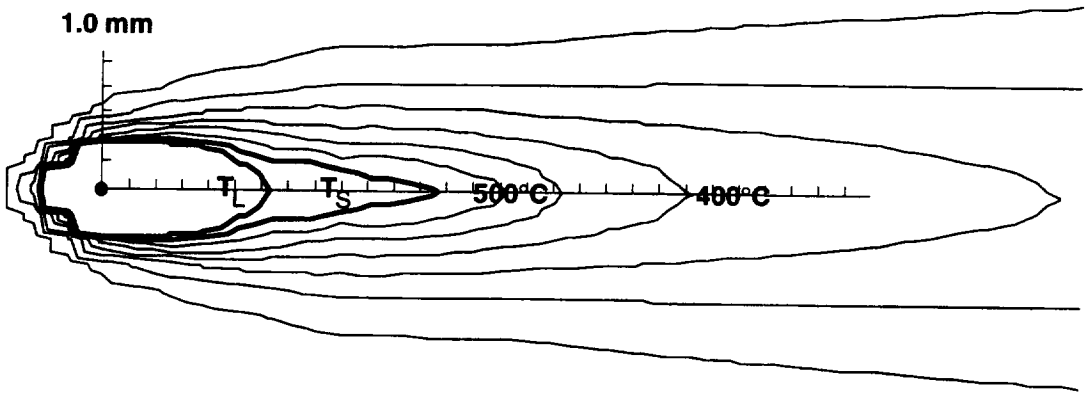

Figure 19 - Simulated Isotherms on the Top Surface During Laser Beam Welding of 2195.

Autogenous

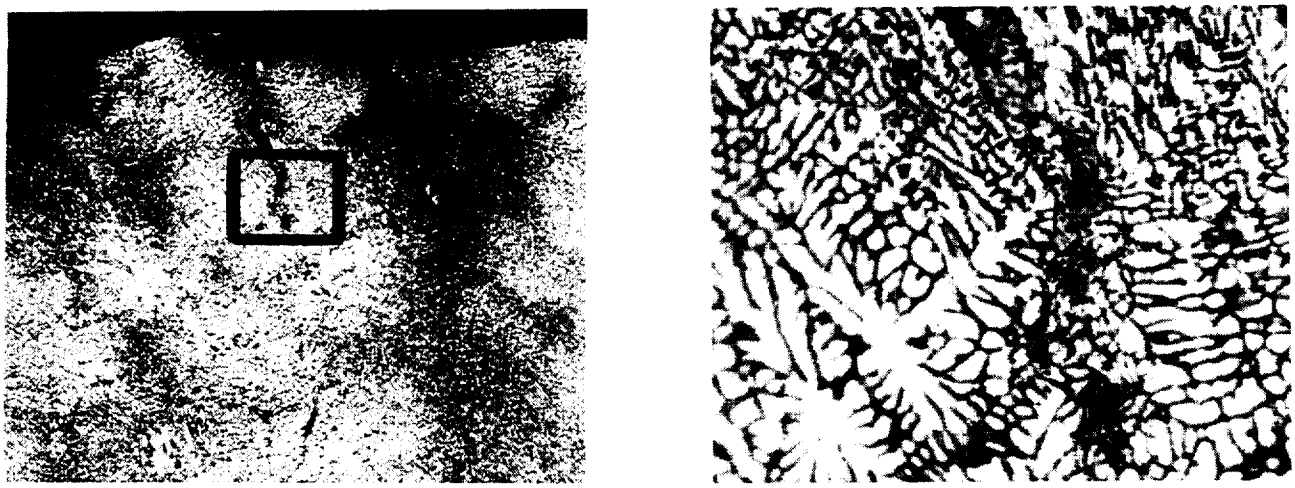

2319 Filler

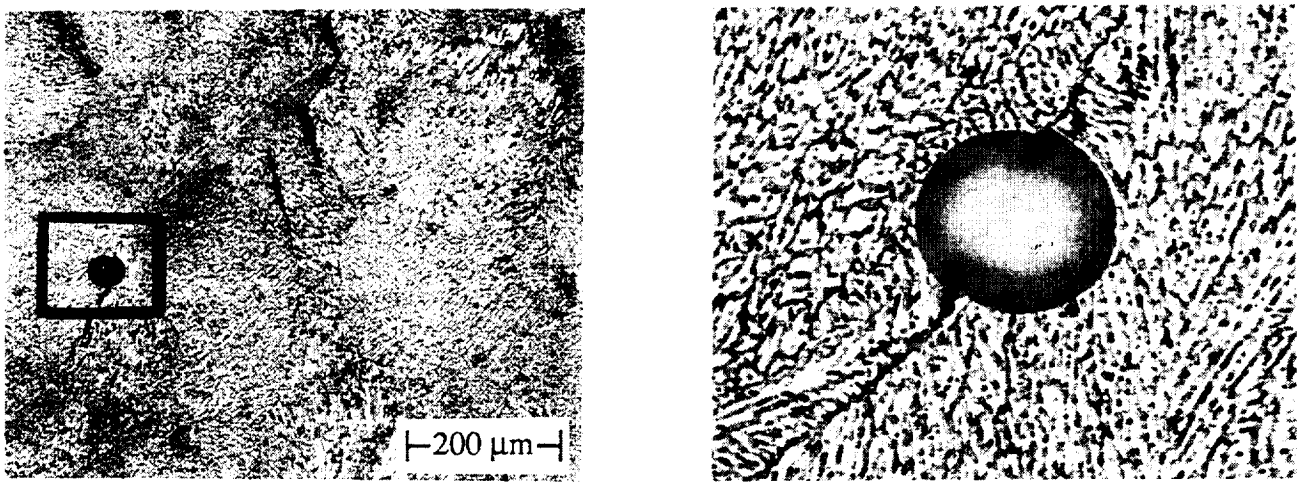

4047 Filler

Figure 20 - Micrographs of Specimens Taken Longitudinally to Weld Centerline for Laser Beam Lap Welds Produced Autogenously and With 2319 and 4047 Filler Alloys.

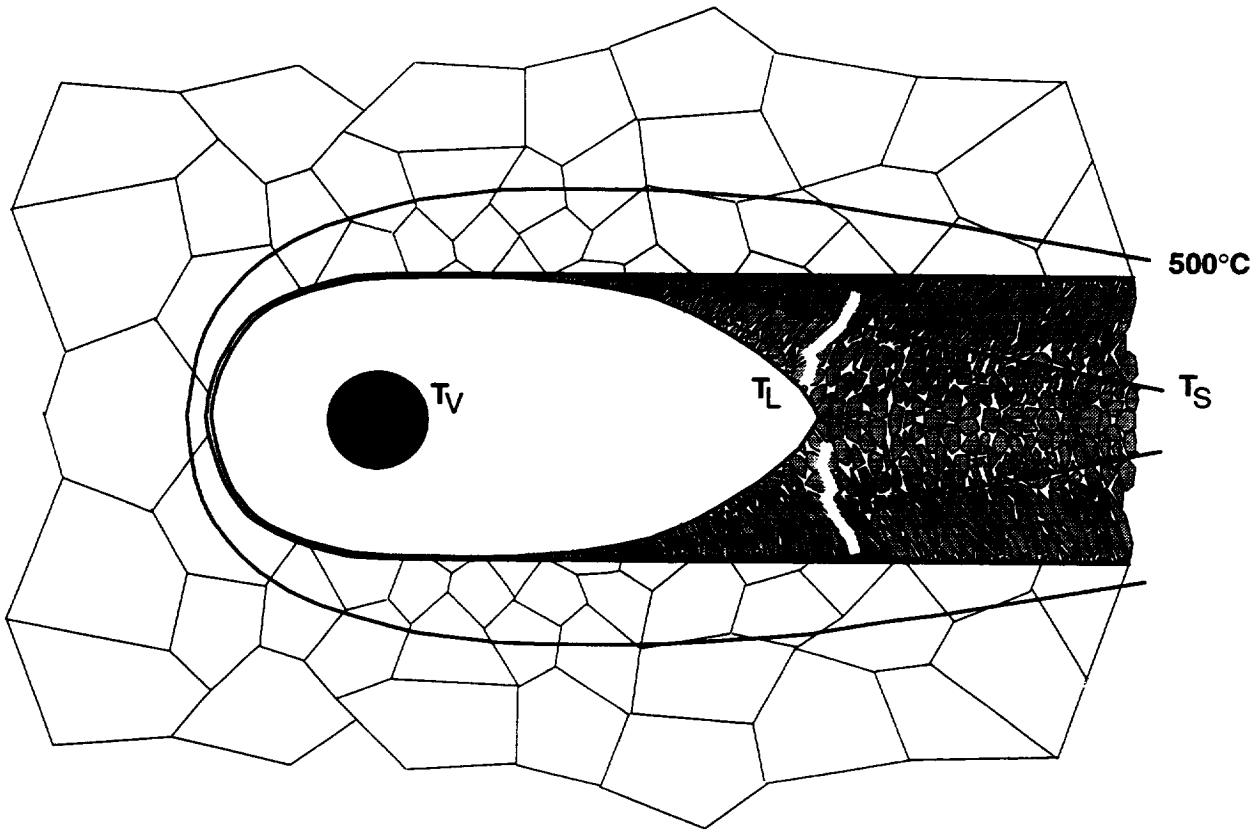

Figure 21 - Composite Schematic of Solidification Cracking of 2195 During Laser Beam Welding.

Aluminum alloys containing Cu and Mg are sensitive to weld metal composition in establishing crack susceptibility. Using experimental alloys representing the Al-Cu-Mg system and ring casting experiments, Pumphrey and Moore was able to show strong correlation between Cu and Mg content with solidification cracking (Ref. 31). This data has been replotted by Cross et al. while adding compositions of several commercial alloys and is shown in Figure 22 (Ref. 32). The composition of alloy 2195 has been added to the graph by the current authors. The figure shows contour lines for different levels of crack sensitivity in terms of total crack length for aluminum alloys containing Cu and Mg. Alloys whose compositions are near the peak crack sensitivity, such as 7075, 8090, 2091 and 2024, possess a great susceptibility to solidification cracking and are extremely difficult to weld. Alloys that are moderately crack sensitive, such as 6061, 2090, 2014, and 2195 may be welded successfully with the aid of filler alloy additions that alter weld chemistry.

The effect of silicon and copper additions to the weld pool on the tendency for aluminum alloys to experience solidification cracking is shown in Figure 23 (Ref. 33). Based on the initial composition of 2195 having 4.0 percent Cu, cracking may be reduced by increasing Si or Cu content of the weld; however, for a given reduction in weld cracking, Si is seen to be a more effective. As an example, to reach a 25.4 mm (1.0 in.) cracking contour line from the starting composition of 4.0 Cu in Figure 22, the weld chemistry must be altered to obtain either 9.0 percent Cu or 3.5 percent Si. Since the highest solute filler alloy containing Cu is 2319 having 6.3 percent nominal Cu content significant reductions in cracking during laser beam welding is not anticipated

with 2319 filler alloy. However, the laser beam welds of 2195 produced with 4047 filler alloy, containing the highest level of Si, resulted in a weld zone having approximately 3.4 percent Cu and 1.0 percent Si (recall Table 4). Increasing the Si content of the weld to 3.5 percent, which should dramatically reduce cracking tendency, would require a filler metal dilution of approximately 30 percent for 4047. Although filler metal dilution at this level is easily attained during conventional welding, the high travel speeds and joint configurations used during laser beam welding hinders the ability to add appreciable amounts of filler metal.

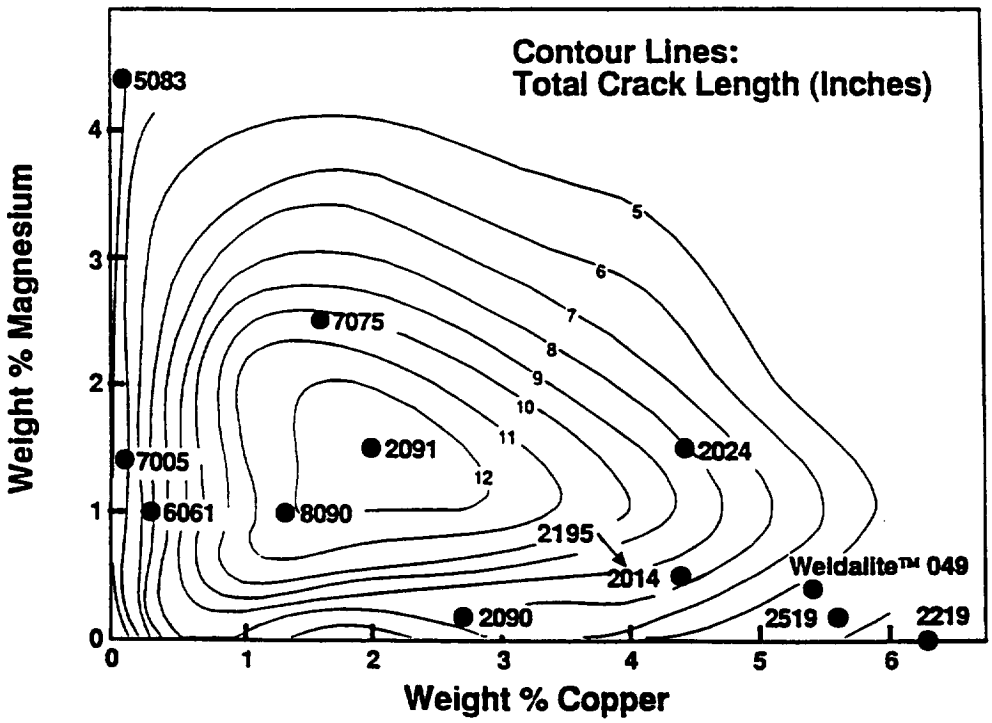

Figure 22 - Solidification Cracking in Terms of Total Crack Length Contours for Aluminum Alloys Containing Copper and Magnesium (Ref. 31&32).

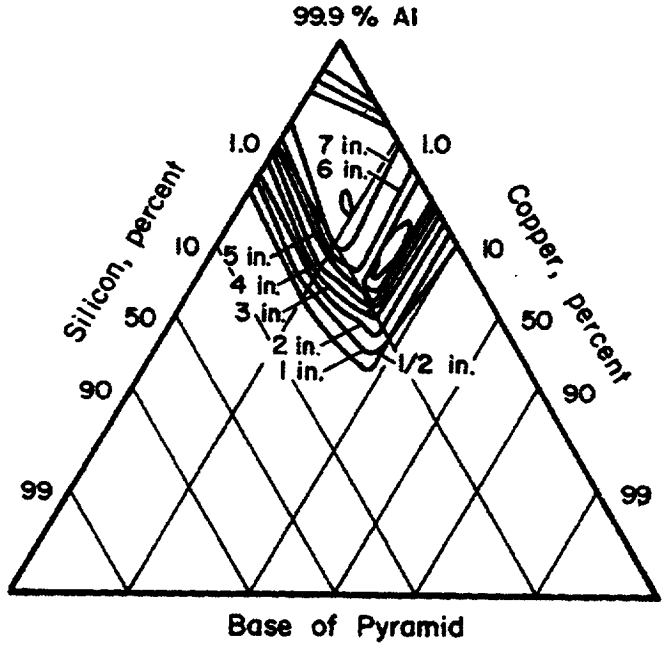

Figure 23 - Solidification Cracking in Terms of Total Crack Length Contours for Aluminum Alloys Containing Copper and Silicon (Ref. 33).

5.3 Second Filler Alloy Experiment

The initial crack sensitivity study showed that cracking could be reduced through the use of Si-containing filler alloys, and analyses of the cracking mechanism and classical theory indicated that Si contents above 3.0 percent should dramatically reduce cracking tendency. Achieving the required dilution of the filler metal to obtain this level of Si would necessitate modifications to process parameters. Evaluations were conducted on the Laser Articulating Robotic System (LARS) to produce lap welds on 1.2 mm (0.050 in.) thick 2195-T6 to 3.1 mm (0.125 in. thick 2195-T8. Material was chemically milled in an aqueous NaOH solution to remove 0.25 mm (0.010 in.) per side prior to welding and the above dimensions represent final thickness after chemical milling. Since considerable time had elapsed between chemical milling and welding (approximately nine-months), specimens were wire-brushed and wiped with acetone just prior to welding. Welds were produced along the center of fully-overlapped panels that were approximately 15 mm (6 in.) in width and 25 mm (10 in.) in length. Initially, filler alloys 4047 (Al-12Si) and 4145 (Al-10Si-4Cu) in 1.15 mm (0.046 in.) diameter were evaluated; however, filler alloy 4047 was found to produce the least amount of cracking and was primarily utilized during the evaluation.

Approximately 40 welds were produced with various parameters. Power output, travel speed, and degree of defocus was altered to maximize the amount of filler metal addition, and hence silicon, within the weld. All welds were inspected visually at 30X magnification to assess the degree of solidification cracking. Parameters that provided the minimal amount of cracking while controlling penetration into the skin-sheet to 50 ± 20 percent were 10.3 kW of power (8.0 kW at the work-piece), 7.9 cm/s (150 IPM) travel speed, stand-off distance of 1.55 mm (0.062 in.) above focus, and a wire feed speed of 15.8 cm/s (300 IPM). All welds were produced with 94.4 l/min. (200 CFH) He for shielding and plume suppression.

Although the frequency of solidification cracks was reduced with parameters that increased the amount of filler addition to the weld, solidification cracking could not be eliminated. It was also noted that the parameters that resulted in increasing levels of filler addition, such as lower travel speed and less defocusing of the beam, were contrary to the parametric window established for optimizing weld profile and pool stability. Inspection of the welded panels produced using the above parameters provided an average of 12 cracks, being transverse to the welding direction and having a length, depth, and morphology identical to those previously reported, along the length of the 25 mm (10 in.) weld. There appeared to be inconsistency in the amount of filler metal dilution, as estimated by the degree of crown reinforcement, along the length of the weld. Areas exhibiting a large weld crown, and hence greater filler metal dilution, exhibited very few weld cracks. The inconsistency in filler metal dilution was believed to be due to slippage of the wire feed drive rolls at relatively high wire feed speeds.

5.4 Summary of Weld Cracking Investigation

Extensive cracking was observed within the fusion zone of autogenous laser beam lap welds of 2195 produced during the reproducibility study. Analyses of the welds indicated that cracking occurred during solidification and could be reduced or eliminated by modification of weld metal composition. Two experiments were conducted to assess the effect of filler alloy additions on crack sensitivity during laser beam welding of 2195. The first experiment was used to ascertain the effects of various filler alloys on cracking and the second experiment involved modification to process parameters for increasing filler metal dilution.

Filler alloys 2319 (Al-6.3 Cu), 4043 (Al-5.3Si), 4047 (Al-12Si), 4145 (Al-10Si-4Cu), and 5356 (Al-5.0Mg) were evaluated for reducing crack sensitivity during laser beam welding of alloy 2195. Autogenous welds were also produced for comparison purposes. Process parameters used during this experiment were a power of 11.0 kW (8.5 kW to the work-piece), 10.6 cm/s (250 IPM) travel speed, stand-off distance of 13.3 cm (5.25 in.), and a wire feed rate of 6.6 cm/s (125 IPM) for the 1.2 mm (0.046 in.) diameter filler wire. These parameters were identical to those established during the parametric study, except for the addition of filler metal. Results indicated that, although filler metal dilution of these welds were less than 10 percent, filler alloys 4047 and 4145 showed promise for eliminating weld cracking. A filler metal dilution of approximately 30 percent for alloy 4047 was estimated to be necessary for eliminating cracking and would result in between 3.0 to 4.0 percent silicon within the weld fusion zone. Dilutions at this level would require modifications to the established process parameters.

Process parameters were established for increasing filler metal dilution but maintaining weld penetration requirements. Parameters that provided the minimal amount of cracking while controlling penetration into the skin-sheet to 50 ± 20 percent were 10.3 kW of power (8.0 kW at the work-piece), 7.9 cm/s (150 IPM) travel speed, stand-off distance of 1.55 mm (0.062 in.) above focus, and a wire feed speed of 15.8 cm/s (300 IPM). Although the frequency of solidification cracks was reduced with parameters that increased the amount of filler addition to the weld, solidification cracking could not be eliminated. It was also noted that the parameters that resulted in increasing levels of filler addition, such as lower travel speed and less defocusing of the beam, were contrary to the parametric window established for optimizing weld profile and pool stability. Visual inspection of these welds indicated that cracking was prevalent in areas exhibiting lower filler metal dilution. Inconsistency in the amount of filler metal dilution, as estimated by the degree of crown reinforcement, was believed to be due to non-uniform wire feed rates.

6.0 TEST SPECIMEN FABRICATION

Although weld cracking was not eliminated, two panels representing laser beam lap-welds were produced using 4047 filler metal for abbreviated mechanical testing. These tests would include testing for tension shear strength at the interface and tensile strength across the partial penetration of the skin. Tests would be conducted at NASA Langley Research Center and entail testing at room temperature and at -196°C (-320°F).

The lap-welds were produced on 1.25 mm (0.050 in.) thick 2195-T6 to 3.12 mm (0.125 in.) thick 2195-T8. Material was chemically milled in a aqueous NaOH solution to remove 0.25 mm (0.010 in.) per side prior to welding and the above dimensions represent final thickness after chemical milling. One panel was produced for obtaining tension shear test specimens, and one panel was produced for obtaining tensile test specimens. Process parameters that resulted in maximum filler metal dilution and penetration of between 30 and 70 percent into the skin were used to produce these panels. These parameters were 10.3 kW of power (8.0 kW at the work-piece), 7.9 cm/s (150 IPM) travel speed, stand-off distance of 1.55 mm (0.062 in.) above focus, and a wire feed speed of 15.8 cm/s (300 IPM). The test panel for obtaining the tension shear specimens were produced by welding along the center of over-lapped sheets being 15.2 cm (6.0 in.) wide and 30.5 cm (12.0 in.) long and having a 10.2 cm (4.0 in.) over-lap. The test panel for obtaining the tensile test specimens were produced by welding along the center of over-lapped sheets being 7.6 cm (6.0 in.) wide and 30.5 cm (12.0 in.) long and being fully over-lapped.

After welding, the panels were visually inspected at 30X magnification and the position of weld cracks were identified. The frequency of cracks were shown to be approximately one crack every 3.0 cm (1.2 in.) of weld length. Sections of weld that did not contain cracks were removed from the tension shear test panel for obtaining test specimens. Ten tension shear test specimens having a nominal width of 0.750 in. were machine from the sections removed from this panel. The top sheet of the panel produced for obtaining tensile strength across the partial penetration weld of the skin was carefully removed by machining. Ten tensile test specimens having a 2.54 cm (1.00 in.) gauge length and a 1.27 cm (0.50 in.) reduced section were machine from the remaining skin. Mechanical property test specimens were forwarded to NASA Langley Research Center for testing.

7.0 SUMMARY

Based on the potential for decreasing costs of joining stiffeners to skin by laser beam welding, a fundamental research program was conducted to address the impediments identified during an initial study involving laser beam welding of aluminum-lithium alloys. Initial objectives of the program were the identification of governing mechanism responsible for process related porosity while establishing a multivariant relationship between process parameters and fusion zone geometry for laser beam welds of alloy 2195 (Al-4.0Cu-1.0Li-0.4Mg-0.4Ag). Specific tasks included: a fundamental characterization of the base material, a parametric study of processing parameters on weld attributes, and a reproducibility study to determine process consistency. The reproducibility study was terminated prior to completion due to the determination of cracks within the welds and necessitated a crack sensitivity investigation concerning filler alloy additions. A 14 kW CO_2 laser and the Laser Articulating Robotic System was used to produce all laser beam welds. The lap-joint configuration utilized during the study entailed welding 1.25 mm (0.050 in.) thick 2195-T6 to 3.12 mm (0.125 in.) thick 2195-T8 and was selected to simulate stiffeners to skin for stiffened panel applications.

Transmission electron microscopy was performed 2195-T8 base material and on specimens removed from various regions of the heat affected zone of variable polarity plasma arc welds. The base metal microstructure of this alloy in the peak aged temper was found to be dominated by T_1 (Al_2CuLi) and θ' (Al_2Cu) precipitates. Both of which form as plates on preferred planes of the matrix. Complete dissolution of θ' occurred within the heat affected zone at temperatures below 220°C (428°F), and partial dissolution of T_1 was observed for peak temperatures of 320°C (608°F). Moderate increases in the size of the T_1 precipitate was detected at peak temperatures approaching 500°C (932°F) and is believed to be caused by growth of partially dissolved precipitate during cooling.

The gradual loss of strength for positions representing these temperature regimes is believed to be attributed to dissolution of the T_1 precipitate. The relatively high peak temperatures associated with positions near the fusion zone interface resulted in complete dissolution of strengthening precipitate and re-precipitation of copper-rich zones upon cooling. The increased strength exhibited within this region is believed to be due to the formation of these zones and, to a lesser degree, solid solution strengthening. A narrow region of the heat affected zone that is adjacent to the fusion zone interface may influence weld toughness by the presence of precipitate free zones and solute depletion.

A three-level fractional factorial experiment was conducted to establish quantitative relationships between primary process parameters and critical weld attributes. The experiment entailed the evaluation of five independent variables (beam power, degree of defocus, travel speed, filler metal, and degree of chemical cleaning) at three levels. The dependent response variables for the evaluation included the width and depth of penetration and radiographic rating for weld soundness. Strong statistical correlation was observed for : weld penetration as a function of welding velocity and stand-off distance, weld width at the interface as a function of stand-off distance, and porosity rating as a function of amount removed by chemical milling and welding velocity. Parameters were identified for maximizing weld width while maintaining adequate penetration and minimizing porosity. These parameters were: an output power of 10 kW, a processing speed of 10.6 cm/s (250 IPM), a stand-off distance of 13.3 cm (5.25 in.), and chemical milling of 0.25 mm (0.010 in.) per side prior to welding.

A reproducibility study using optimal parameters was conducted to assess process consistency during laser beam welding based on the parameters established from the factorial experiment. Although weld consistency appeared high for welds produced during partial completion of this study, numerous cracks on the top-surface of the welds were discovered during visual inspection. The reproducibility study was terminated until methods to eliminated weld cracking could be identified.

A crack sensitivity study was performed to identify possible means of reducing or eliminating cracks within the laser beam welds of 2195. Analyses of the welds indicated that cracking occurred during solidification and could be reduced or eliminated by modification of weld metal composition. Two experiments were conducted to assess the effect of filler alloy additions on crack sensitivity during laser beam welding: the first experiment was used to ascertain the effects of various filler alloys on cracking and the second experiment involved modification to process parameters for increasing filler metal dilution.

Filler alloys 2319 (Al-6.3 Cu), 4043 (Al-5.3Si), 4047 (Al-12Si), 4145 (Al-10Si-4Cu), and 5356 (Al-5.0Mg) were evaluated for reducing crack sensitivity. Autogenous welds were also produced for comparison purposes. Process parameters used during this experiment were identical to those established during the parametric study, except for the addition of filler metal. Results indicated that filler alloys 4047 and 4145 showed promise for eliminating weld cracking. A filler metal dilution of approximately 30 percent for alloy 4047 was estimated to be necessary for eliminating cracking and would result in between 3.0 to 4.0 percent silicon within the weld fusion zone. Dilutions at this level would require modifications to the established process parameters.

Process parameters were established for increasing filler metal dilution but maintaining weld penetration requirements. Parameters that provided the minimal amount of cracking while controlling penetration into the skin-sheet to 50 ± 20 percent were 10.3 kW of power (8.0 kW at the work-piece), 7.9 cm/s (150 IPM) travel speed, stand-off distance of 1.55 mm (0.062 in.) above focus, and a wire feed speed of 15.8 cm/s (300 IPM). Although the frequency of solidification cracks was reduced with parameters that increased the amount of filler addition to the weld, solidification cracking could not be eliminated. It was also noted that the parameters that resulted in increasing levels of filler addition, such as lower travel speed and less defocusing of the beam, were contrary to the parametric window established for optimizing weld profile and pool stability. Visual inspection of these welds indicated that cracking was prevalent in areas exhibiting lower filler metal dilution. Inconsistency in the amount of filler metal dilution, as estimated by the degree of crown reinforcement, was believed to be due to non-uniform wire feed rates.

Although weld cracking was not eliminated, two panels representing laser beam lap-welds were produced using 4047 filler metal and the modified process parameters for abbreviated mechanical property tests. These tests, to be performed at NASA Langley Research Center, would include testing for tension shear strength at the interface and tensile strength across the partial penetration of the skin. Mechanical property specimens were obtained from weld areas that did not exhibit cracking based on visual inspection and forwarded to NASA Langley Research Center.

8.0 ACKNOWLEDGEMENTS

The authors would like to acknowledge the assistance of Mr. J. F. Tressler and Mr. W. G. Rhoads of the Applied Research Laboratory in performing the laboratory trials and Ms. C. L. Lach of NASA Langley Research Center for technical support thoughout this program.

9.0 REFERENCES

1. Martukanitz, R. P. and K. G. Lysher, The Feasibility of Producing Aluminum-Lithium Structures for Cryogenic Tankage Applications by Laser Beam Welding, Technical Memorandum prepared under Contract Number N00039-88-C-0051 for NASA Langley Research Center, Applied Research Center, The Pennsylvania State University, P. O. Box 30, State College, Pa. (1993).

2. Wefers, K. and F. A. Mozelewski, Aluminium, March (1988).

3. Dickenson, R. C., Wefers, K., and Lawless, K. R., Proceedings of the Fifth International Aluminum-Lithium Conference, Materials and Component Engineering Publications Ltd., Birmingham (UK), 1337 (1989).

4. Bavarian, B., Becker, J., Parikh, S. N., and Zamanzadeh, M, Proceedings of the Fifth International Aluminum-Lithium Conference, Materials and Component Engineering Publications Ltd., Birmingham (UK), 1231 (1989).

5. Hardy, D. J., Undergraduate Research Thesis, Materials Science Department, The Pennsylvania State University, University Park, Pa. (1993).

6. Martukanitz, R. P., Lysher, K. G., and Howell, P. R., NASA Conference Publication 3287, 237 (1994).

7. Marsico, T. A. and Kossowsky, R, Proceedings of the Fifth International Aluminum-Lithium Conference, Materials and Component Engineering Publications Ltd., Birmingham (UK), 1447 (1989).

8. Katayama, S., Lundin, C. D., Danko, J. C., and McKay, T. D., Conference Proceedings of Recent Trends in Welding Science and Technology, ASM, 687 (1990).

9 Martukanitz, R. P. and Smith, D. J., Sixth International Conference on Aluminum Weldments, American Welding Society, Miami, 309 (1995).

10. Silcock, J. M., J. Inst. Metals., Vol. 88, 357 (1959).

11. Noble, B. and Thompson, G. E., Met. Sci. Jour., Vol. 6, 167 (1972).

12. Rioja, R. J. and Ludwiczak, E. A., Proceedings of Aluminum-Lithium III, The Institute of Metals, London, 471 (1986).

13. Tosten, M. H., Vasudevan, A. K., and Howell, P. R., Proceedings of Aluminum-Lithium III, The Institute of Metals, London, 483 (1986).

14. Huang, J. C. and Ardell, A. J., Mat. Sci. and Tech., Vol. 3, 176 (1987).

15. Sanders, T. H., Jr. and Starke, E. A. Jr., Proceedings of Fifth International Aluminum-Lithium Conference, Materials and Component Engineering Publications Ltd., Birmingham, UK, 1 (1989).

16. Pickens, J. R., Heubaum, and Langan, T. J., Proceedings of 30th CIM Conference of Metallurgists, CIM, 3, (1991).

17. Ringer, S. P., Hono, K. Polmear, I. J., and Sakurai T., Proceedings of Solid→Solid Phase Transformations, TMS, 165 (1995).

18. Martukanitz, R. P. and Howell, P. R., Proceedings of the World Trends in Welding Research, ASM International, Materials Park, (1995)

19. Shabel, B. and Young, R. F., Proceedings of Nondestructive Characterization of Materials, Plenum Press, New York, 335 (1987).

20. Gayle, F. W., Heubaum, F. H., and Pickens, J. R., Proceedings of Fifth International Aluminum-Lithium Conference, Materials and Component Engineering Publications Ltd., Birmingham, UK, 701 (1989).

21. Williams, D. B. and Edington, J. W., J. Microsc., Vol. 108, 113 (1976).

22. Jha, S. C., Sanders, T. H., and Dayananda, M. A., Acta. Met., Vol. 35, 473 (1987).

23. Noble, B, Harris, S. J., and Dinsdale, K., Metal Sci., Vol. 16, 425 (1982).

24. Huang, J. C. and Ardell, A. J., Acta. Met., Vol. 36, 2995 (1988).

25. Kocks, U. F., Physics of Strength and Plasticity, MIT Press, Cambridge, Ma., 143 (1969).

26. Huang, J. C. and Ardell, A. J., Proceedings of the 4th International Aluminum-Lithium Conference, Les Editions de Physicue, Les Ulis, France, C3-373 (1987).

27. Suresh, S. Vasudevan, A. K., Tosten, M., and Howell, P. R., Acta. Met., Vol. 35, 25 (1987).

28. Zamiski, G. F. and Ono, K., Proceedings of Fifth International Aluminum-Lithium Conference, Materials and Component Engineering Publications Ltd., Birmingham, UK, 869 (1989).

29. U.S. Department of Commerce, Experimental Statistics (Handbook 91), 2-12 (1963).

30. Box, G. E. P. and Behnken, D. W., Technometrics, Vol. 2, 455, November (1960).

31. Pumphrey, W. I. and Moore, D. C., Journal of the Institute of Metals, Vol. 73, 425 (1948).

32. Cross, C. E., Tack, W. T., Loechel, L. W., and Kramer, L. S., Proceedings of the Conference on Weldability of Materials, Eds. R. Patterson and K. Mahin, ASM International, 275 (1990).

33. Redstone Arsenal, Metals Progress, Vol. 76, 116, July (1959).

REPORT DOCUMENTATION PAGE

Form Approved
OMB No. 0704-0188

1. AGENCY USE ONLY (*Leave blank*)	2. REPORT DATE	3. REPORT TYPE AND DATES COVERED
	September 1996	Contractor Report

4. TITLE AND SUBTITLE
A Fundamental Study of Laser Beam Welding Aluminum-Lithium Alloy 2195 for Cryogenic Tank Applications

5. FUNDING NUMBERS
G NAG1-1554
WU 505-63-50-02

6. AUTHOR(S)
R. P. Martukanitz
R. Jan

7. PERFORMING ORGANIZATION NAME(S) AND ADDRESS(ES)
Applied Research Laboratory
The Pennsylvania State University
P.O. Box 30
State College, PA 16804

8. PERFORMING ORGANIZATION REPORT NUMBER
95-41

9. SPONSORING / MONITORING AGENCY NAME(S) AND ADDRESS(ES)
National Aeronautics and Space Administration
Langley Research Center
Hampton, VA 23681-0001

10. SPONSORING / MONITORING AGENCY REPORT NUMBER
NASA CR-201614

11. SUPPLEMENTARY NOTES
This report was prepared for NASA Langley Research Center (LaRC) under a grant between LaRC and the Applied Research Laboratory of Pennsylvania State University. Langley Technical Monitor: Cynthia L. Lach.

12a. DISTRIBUTION / AVAILABILITY STATEMENT
Unclassified - Unlimited
Subject Category - 29

12b. DISTRIBUTION CODE

13. ABSTRACT (*Maximum 200 words*)

Based on the potential for decreasing costs of joining stiffeners to skin by laser beam welding, a fundamental research program was conducted to address the impediments identified during an initial study involving laser beam welding of aluminum-lithium alloys. Initial objectives of the program were the identification of governing mechanism responsible for process related porosity while establishing a multivariant relationship between process parameters and fusion zone geometry for laser beam welds of alloy 2195. A three-level fractional factorial experiment was conducted to establish quantitative relationships between primary laser beam processing parameters and critical weld attributes. Although process consistency appeared high for welds produced during partial completion of this study, numerous cracks on the top-surface of the welds were discovered during visual inspection and necessitated additional investigations concerning weld cracking. Two experiments were conducted to assess the effect of filler alloy additions on crack sensitivity: the first experiment was used to ascertain the effects of various filler alloys on cracking and the second experiment involved modification to process parameters for increasing filler metal dilution. Results indicated that filler alloys 4047 and 4145 showed promise for eliminating cracking.

14. SUBJECT TERMS
Laser Welding
Aluminum-lithium alloys 2195
Built-up structure

15. NUMBER OF PAGES
47

16. PRICE CODE
A03

17. SECURITY CLASSIFICATION OF REPORT	18. SECURITY CLASSIFICATION OF THIS PAGE	19. SECURITY CLASSIFICATION OF ABSTRACT	20. LIMITATION OF ABSTRACT
UNCLASSIFIED	UNCLASSIFIED		